CHAPTER 4
UNREINFORCED AND GEOCELL-REINFORCED SAND BED UNDER STATIC LOADS

4.1 Introduction

In this chapter, the results obtained from the model tests on unreinforced and geocell-reinforced sand beds subjected to static loads are presented and discussed. Three different types of footings (i.e. square, rectangular, and strip footing) were used to investigate the effect of the shape of footing on unreinforced and geocell-reinforced sand beds. Besides, the influence of various parameters such as relative density of sand subgrade, geocell pocket size, geocell height, geocell reinforcement width, and relative density of infill sand in the geocells was studied to understand the efficacy of geotextile-based geocell reinforcement under square footing to achieve the maximum performance benefits. Thirty-nine numbers of different model tests (test series A, B1, C1, D1, E1, F1, G1, H, and I) were conducted in this research. The test series details are presented in Table 3.4.

Figs. 4.1a, 4.1b, and 4.1c show a strip (width B), a square ($B \times B$), and a rectangular ($B \times$ length L) foundation being supported by sand which is reinforced with a geocell layer. The top layer of the geocell is located at a depth u measured from the bottom of the foundation. The equivalent diameter of the geocell pocket size is d. The height of the geocell reinforcement layer is h. The width of the geocell layer under the strip foundation is b, and those under the square and rectangular foundations measure $b \times b$ and $b \times l$ respectively.

The test results are discussed in terms of footing settlements (s) and surface deformations (δ) of the ground concerning bearing pressure. The parameters such as footing settlements and surface deformations of the ground are normalized with the width of the footing (B) to express them in a non-dimensional form as s/B (%) and δ/B (%), respectively. In literature (Boiko & Alhassan [14], Cerato & Lutenegger [17]), it is found that the ultimate bearing pressure of unreinforced soil generally occurs at a settlement ratio of 5% to 10% of the footing width. Therefore, in this study, the ultimate bearing capacity of unreinforced and reinforced soil has been considered as s/B = 10%.

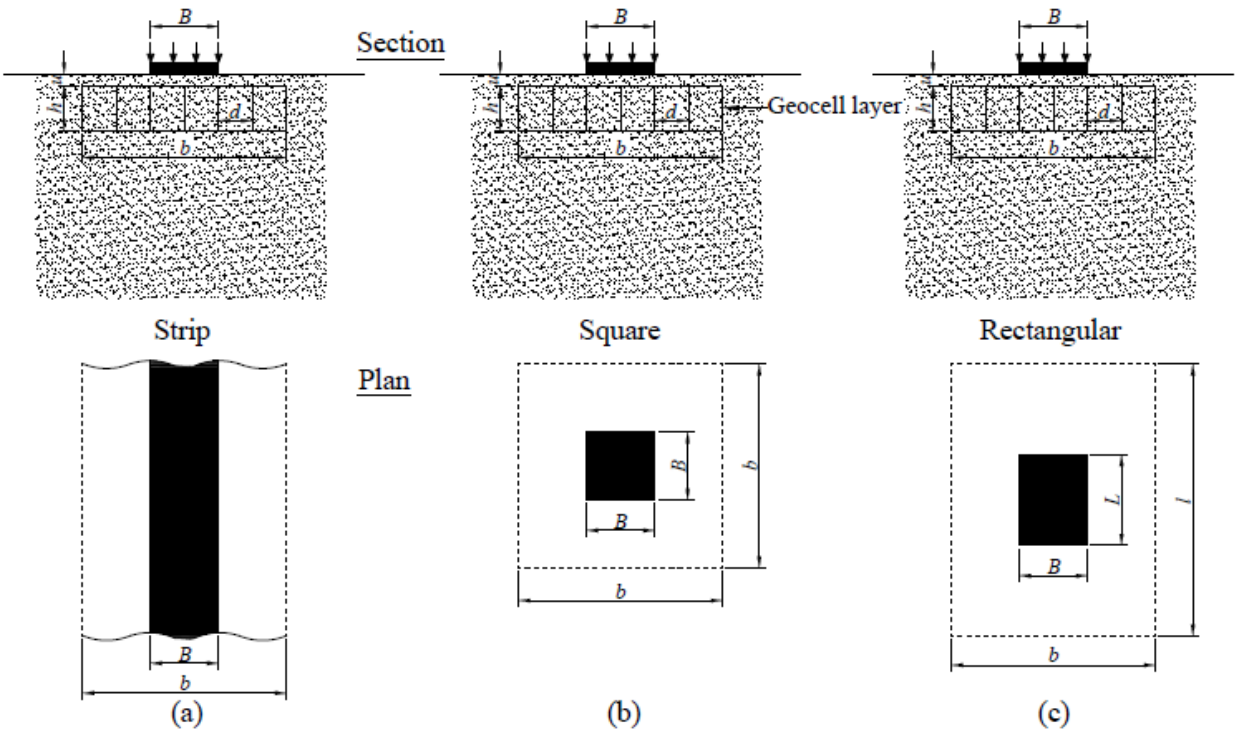

Fig. 4.1 Strip, square and rectangular foundations supported by geocell-reinforced sand

4.2 Unreinforced sand beds

The ultimate bearing capacity (q_U) for unreinforced surface foundations on dry sand can be expressed by conventional formula (Vesic [132]) as

$$q_U = q_{U(\mathrm{st})} = 0.5\gamma_d B N_\gamma \quad \text{for strip foundation} \tag{4.1}$$

$$q_U = q_{U(\mathrm{sq})} = 0.4\gamma_d B N_\gamma \quad \text{for square foundation} \tag{4.2}$$

and

$$q_U = q_{U(\mathrm{rec})} = 0.5\gamma_d B N_\gamma (1 - 0.4\frac{B}{L}) \quad \text{for rectangular foundation} \tag{4.3}$$

where $q_{U(\mathrm{st})}$, $q_{U(\mathrm{sq})}$, and $q_{U(\mathrm{st})}$, are the ultimate bearing capacity of the strip, square and rectangular foundations, respectively; γ_d is the dry unit weight of soil; and N_γ is the bearing capacity factor. The variation of footing settlement with bearing pressure for three different types of footings (i.e., square, rectangular, and strip) on unreinforced sand beds having a relative density of 70% are presented in Fig. 4.2. It can be seen from the curves

that the experimental ultimate bearing capacities of square, rectangular and strip footings are determined as 91 kPa, 105 kPa, and 145 kPa, respectively at measured settlement *s/B* = 10%.

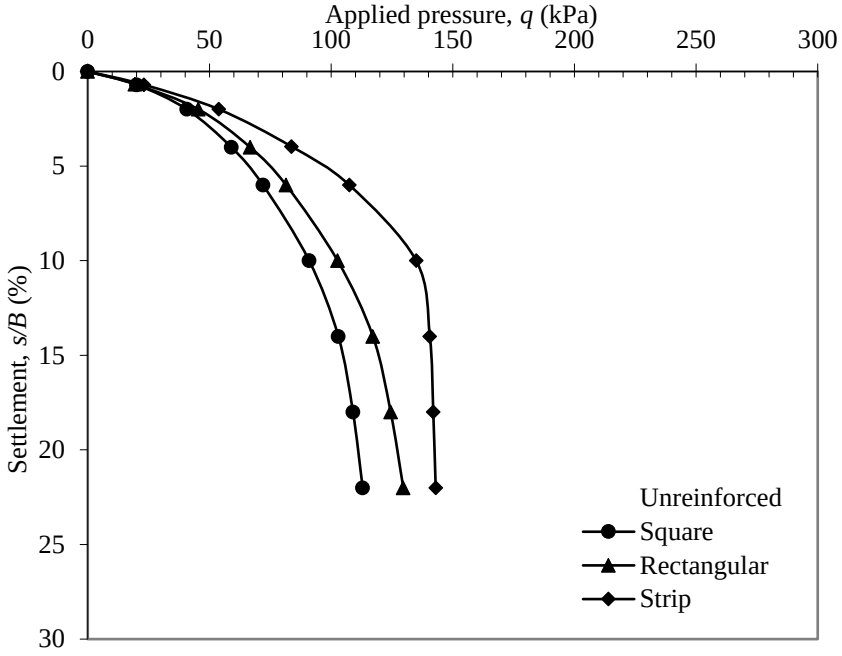

Fig. 4.2 Variation of footing settlement with bearing pressure for different shapes of footing supported on unreinforced sand beds.

The load-settlement curves also show that the failure modes are local failures for both square and rectangular types of footings. However, the mode of failure changes to a general type of failure showing a definite peak in the case of strip footing (plane strain condition). Further, it is clear from the figure that as *B/L* (*L*- length of footing) increases from strip footing (plane strain) to square footing, the peak value of bearing pressure becomes less conspicuous. This result suggests that in the 3D case, (i.e. square and rectangular footing) the failure of ground outside the footing area is more progressive than in the plane strain case (i.e. strip footing). In the case of square and rectangular footing ($B/L > 0.0$), unlike the plane strain case of strip footing, the post-peak curves never fall abruptly. This may be attributed to the different ways of strain localization on the ground for both the 3D and 2D cases.

As discussed in the previous chapter (Chapter 3), the φ value was determined by the direct shear test. However, an adjustment of φ_{ps} to φ_{tr} is recommended (Bowles [15]) for $L/B < 2$

(and in this model tests $L/B = 1$ & $1.33 < 2$ for square and rectangular footings) because the soil wedge beneath the footing base is much closer to a triaxial state than plane strain state. Otherwise, the use of φ_{ps} instead of φ_{tr} is recommended if $L/B > 2$ (for strip footing) due to a plane strain state.

Lade & Lee [68] proposed the angle of shearing resistance of coarse-grained soils from the plane strain state (φ_{ps}) as follows-

$$\varphi_{ps} = 1.5\varphi_{tr} - 17 \qquad (\varphi_{tr} > 34^0) \tag{4.4}$$

$$\varphi_{ps} = \varphi_{tr} \qquad (\varphi_{tr} \leq 34^0) \tag{4.5}$$

The theoretical values of q_U are calculated by using eq.4.1, eq.4.2, and eq.4.3. The calculation details are shown in *Appendix 1*. The theoretical ultimate bearing capacity of these foundations is obtained as $q_{U(\text{st})}$ = 145 kPa, $q_{U(\text{sq})}$ = 80 kPa, and $q_{U(\text{rec})}$ = 70 kPa for strip, square, and rectangular footing respectively.

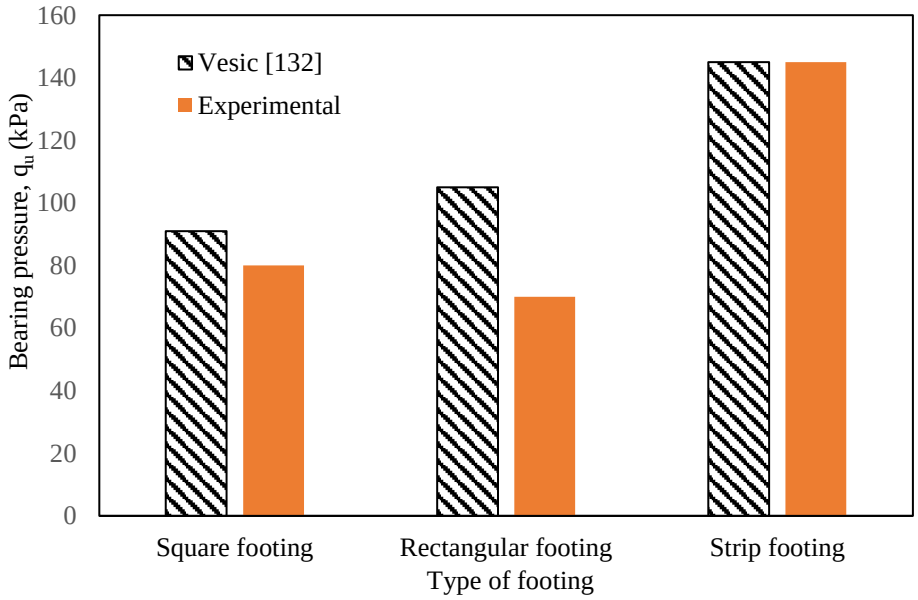

Fig. 4.3 Comparison of theoretical and experimental ultimate bearing pressure for different types of footings

The results suggest a good agreement between the theoretical and experimental values for strip and square footings (Fig. 4.3).

Fig. 4.4 shows the relationships between the shape factor and *B/L* ratio. The model test results are compared with the existing theoretical and empirical formulas (De Beer [30], Hansen [39], Meyerhof [88],. The first approach is a semi-empirical method put forth by Meyerhof [88],

$$S_\gamma = 1 + 0.1\ tan^2(45 + \frac{\varphi}{2})\frac{B}{L} \tag{4.6}$$

The second approach is a semi-empirical one presented by De Beer [30], derived from his 1g small-scale model tests,

$$S_\gamma = 1 - 0.4\frac{B}{L} \tag{4.7}$$

The calculation of the shape factor, s_γ for Fig. 4.4 is shown in *Appendix 2*.

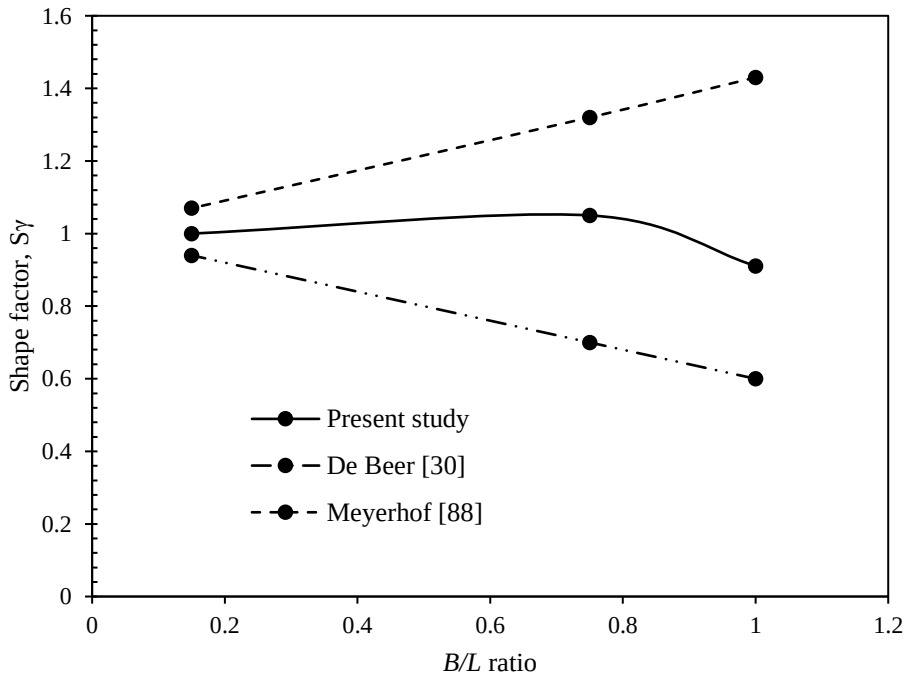

Fig. 4.4 Effect of shape factors

The comparison shown in Fig. 4.4 is consistent with De Beer [30] however, it shows a reverse trend to the relation of Eq. 4.1 provided by Meyerhof [88].

The surface deformation profiles for the three different types of footings (square, rectangular, and strip) are shown in Fig. 4.5a-c. The distance from the footing centre '*x*' is expressed in non-dimensional form as *x/B*. The surface settlement and heave are differentiated with the '-' and '+' sign, respectively. The variation of average surface deformations (δ) concerning footing settlement at a distance $x = 1.5B$ from the centre of the footing, are depicted in Figs. 4.6. It can be seen that heaving is more predominant for strip footing, as compared to square and rectangular footings. Further, the surface deformations are mostly pronounced around the footing centre or centre line (at $x = 1.5B$); while it is reduced to zero as the distance increase at $x = 3B$. The results show that the surface heaving (δ/B) increases from 1.4 to 2.6 for strip footing, whereas it is about 1.2 to 2 for square footing and about 1.3 to 2.1 for rectangular footing when footing settles down from 6 to 10% of footing width, *B*. Thus, the test results indicate that the surface heaving reduces as *B/L* increases from 0.0 (plane strain) i.e., maximum heaving for strip footing and minimum heaving for the square type of footing.

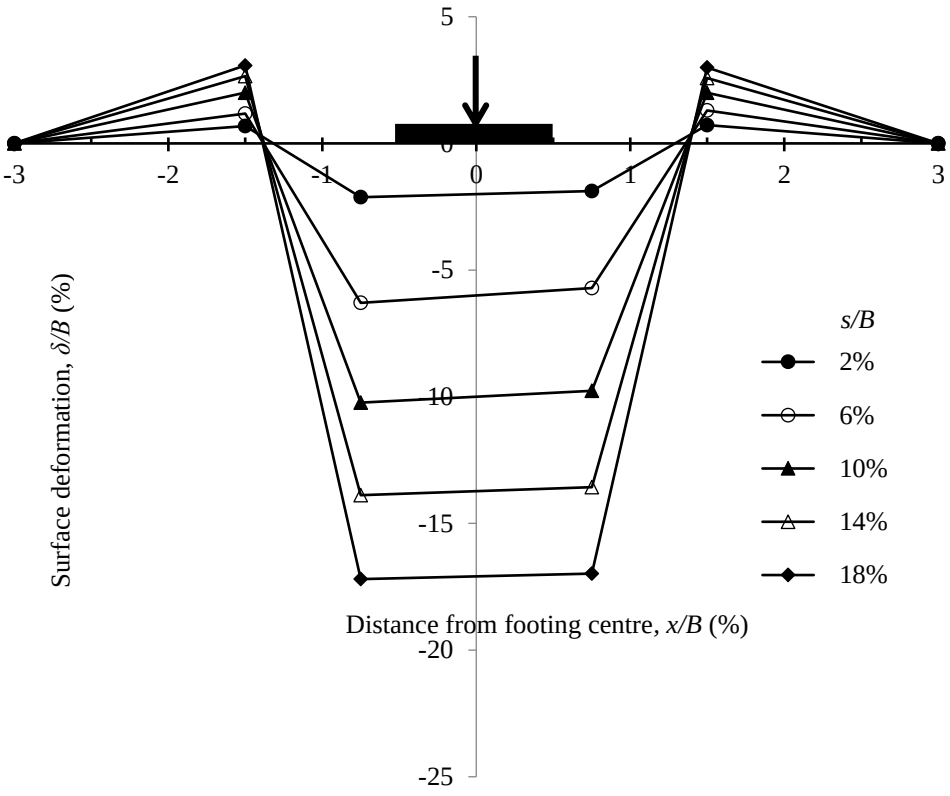

(a)

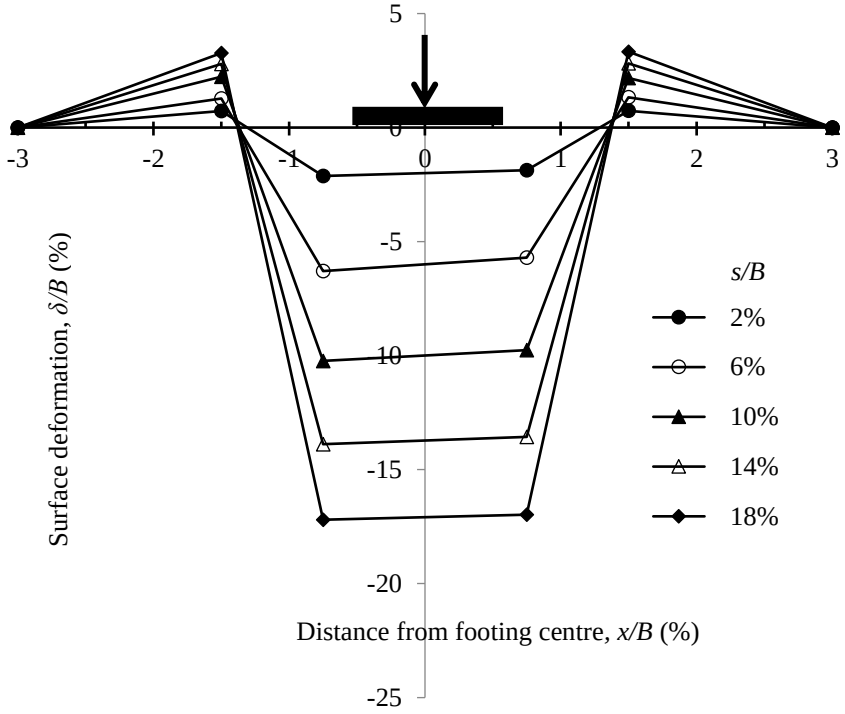

(b)

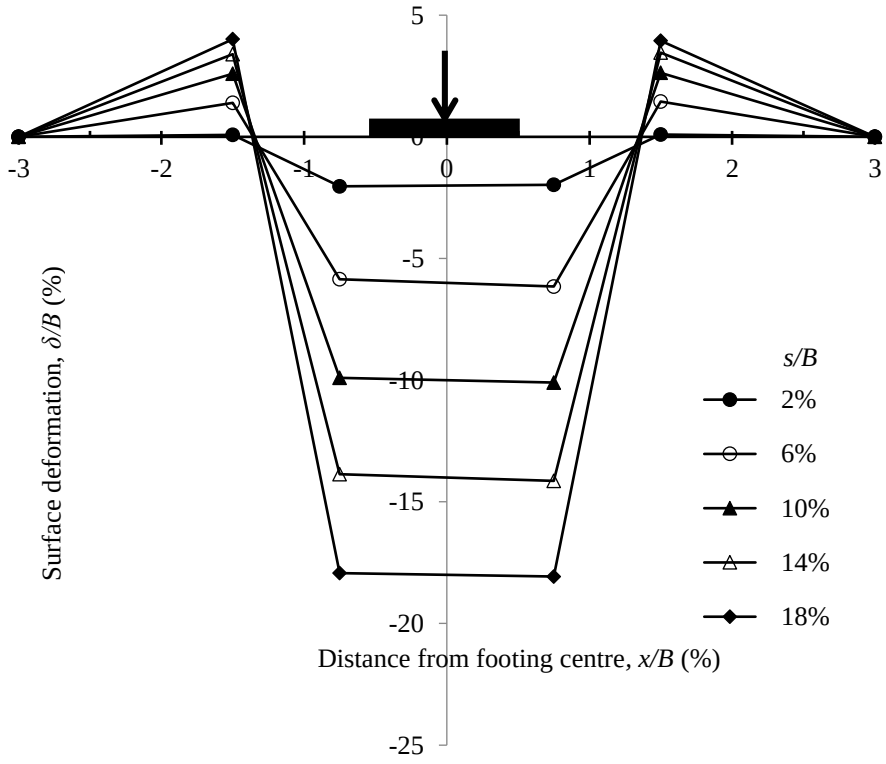

(c)

Fig. 4.5 Surface heaving with footing settlement for unreinforced sand beds: (a) square footing; (b) rectangular footing; (c) strip footing

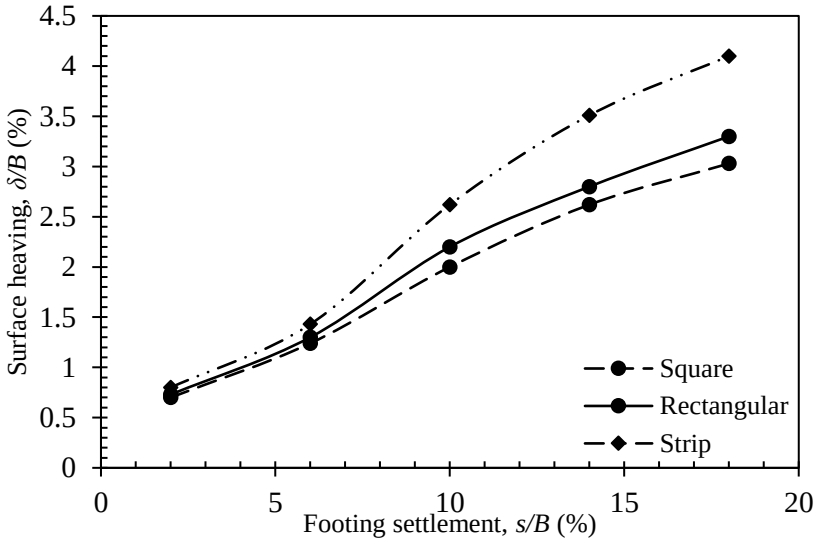

Fig. 4.6 Variation of δ/B with s/B at $x = 1.5B$ for unreinforced sand beds of different types of footings

Fig. 4.7 shows the relationship between the applied pressure and the normalized settlement for square footing on unreinforced sand beds with three different relative densities (D_r = 35, 70, and 90%).

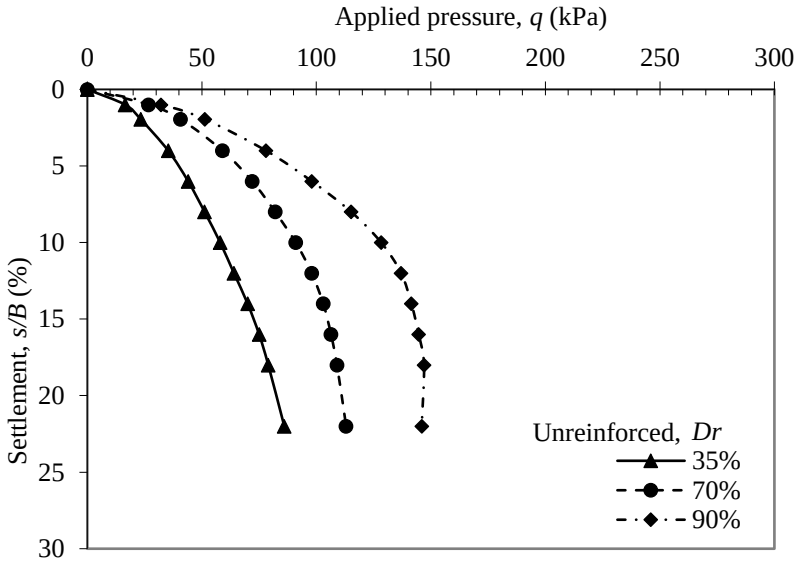

Fig. 4.7 Variation of footing settlement with bearing pressure for different relative densities of unreinforced sand beds.

It can be seen from the curve in Fig. 4.7 that the ultimate load-carrying capacity is about 58 kPa for D_r = 35% and about 128 kPa for D_r = 90% at measured settlement s/B = 10% as summarized in Table 4.1.

Table 4.1 Summary of load-settlements results for different relative densities of unreinforced sand

Footing settlements (*s/B*)	Load intensity (kN/m^2)		
	D_r = 35%	D_r = 70%	D_r = 90%
10%	**58.0**	**91.0**	**128.3**

The results shown in Fig. 4.7 suggest that sand beds with higher relative density result in greater bearing pressure response against footing settlement. It is also noted that the bearing capacity failure for dense sand (D_r = 90%) has taken place at a settlement equal to 12% of the footing width. Moghaddas Tafreshi and Dawson [90] have also observed the same range of settlement ratio, *i.e. s/B* = 12% for the bearing capacity failure of the unreinforced sand bed. The curves for unreinforced sand foundations also clearly indicate the punching shear failure, the local shear failure, and general shear failure for relative densities of 35, 70, and 90%, respectively. A similar trend of observation was also reported by Vesic [132] for a model footing supported on an unreinforced sand bed. Moreover, it can be seen that the variations of bearing pressure with footing settlements are non-linear, and well-defined failure surfaces are seen for all three sand beds within the range of settlements tested (up to *s/B* = 22%). The results also revealed that at normalized settlement of 2%, the load-carrying capacity for loose sand bed (D_r = 35%) is 23 kPa, whereas it is 51 kPa for the dense sand (D_r = 90%). The corresponding values for 12% settlements were 64 kPa and 137 kPa, respectively.

The surface deformation profiles for relative densities of 35%, 70%, and 90% are shown in Fig. 4.8a-c. The distance from the footing centre '*x*' is expressed in non-dimensional form as *x/B*. The surface settlement and heave are differentiated with the '-' and '+' sign, respectively. The progression of the settlement or heaving for each increment can be tracked using the figures. It can be seen that heaving is more predominant for a relative density of 70% and 90%, as compared to the relative density of 35% in an unreinforced sand bed. Further, the surface deformations are mostly pronounced around the footing centre (at $x = 1.5B$); while it is reduced to zero as the distance increase at $x = 3B$.

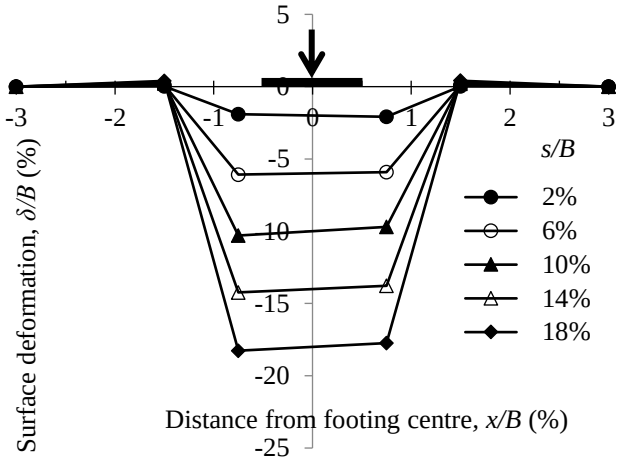

(a)

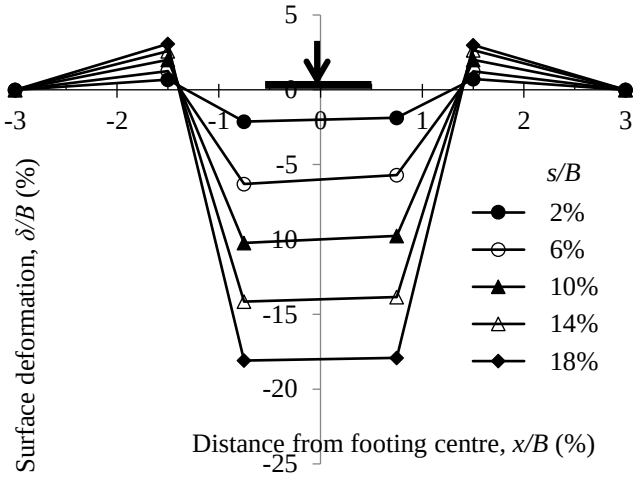

(b)

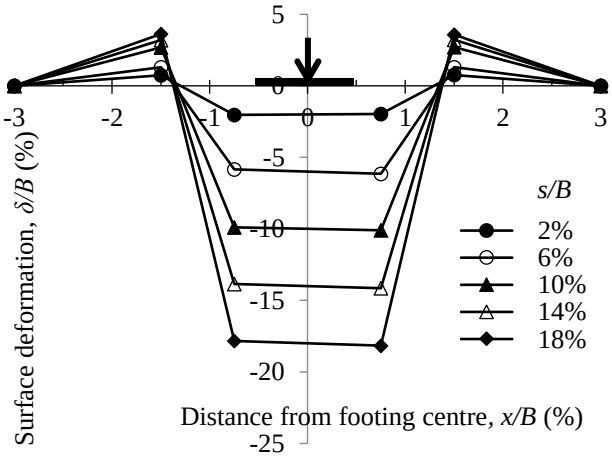

(c)

Fig. 4.8 Surface heaving with footing settlement for unreinforced sand beds: (a) unreinforced, D_r = 35%; (b) unreinforced, D_r = 70%; (c) unreinforced, D_r = 90%.

The variation of average surface deformations (δ) concerning footing settlement at a distance $x = 1.5B$ from centre of the footing, are depicted in Fig. 4.9. The results show that the surface heaving (δ/B) increases from 1.3 to 2.7 for unreinforced sand with $D_r = 90\%$ when footing settles down from 6 to 10% of footing width, B.

A similar trend is also observed for the unreinforced foundation soils with $D_r = 70\%$. But, in this case, the surface heaving (δ/B) is 1.24 to 2.0 in the measured settlement of 6 to 10% of footing width. It is also to be noted that since a punching shear failure has taken place in unreinforced soil with $D_r = 35\%$ (Fig. 4.7), therefore, the surface heaving at $s/B = 10\%$ is about 0.2% only. The increased surface heaving for the unreinforced sand beds with D_r = 70 and 90% is due to the effect of the dilatant behavior of dense sand.

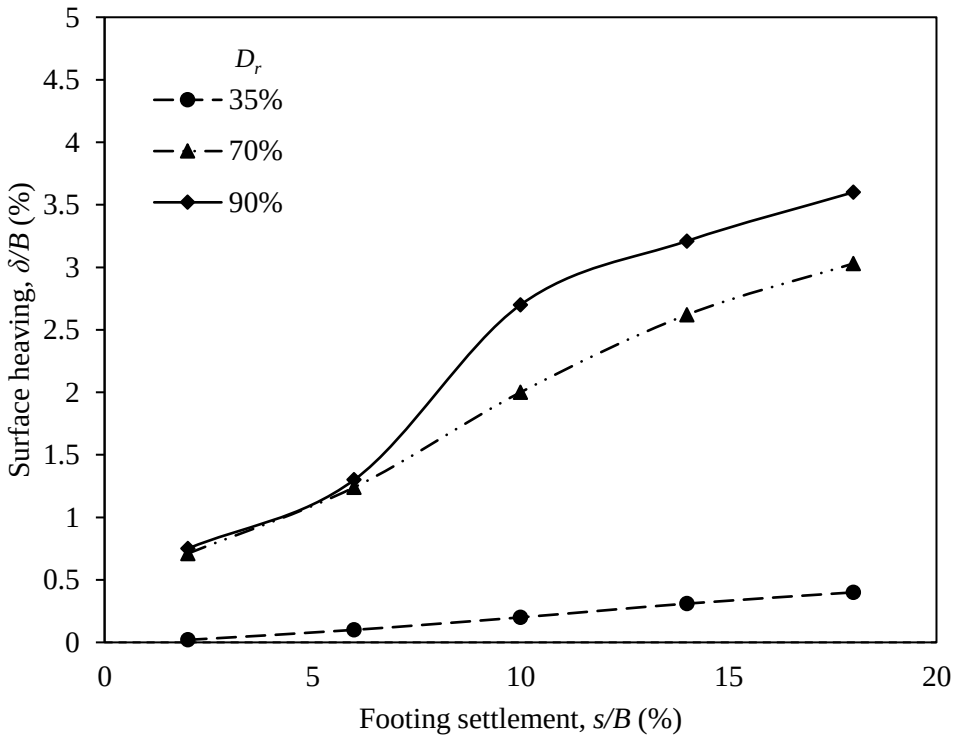

Fig. 4.9 Variation of surface deformations at $x = 1.5B$ for unreinforced sand beds of different relative densities.

A comparison of theoretical ultimate bearing pressure (Hansen [39], Meyerhof [85], Terzaghi [129], Vesic [132]) with the maximum bearing pressures obtained from the experiments is presented in Table 4.2 and plotted in Fig. 4.10. The ultimate bearing capacity of square footing on the surface of homogeneous sand bed is estimated by eq. 4.2.

Table 4.2 Calculated values of ultimate bearing capacities q_U by Terzaghi [129], Meyerhof [85], Hansen [39], and Vesic [132] for centric vertical condition along with present experimental values from test series B1 (Table 3.4)

State of sand	γ (kN/m^3)	D_r (%)	φ_{tr}, (Eq. 4.4 & 4.5) (degree) (*Appendix 1*)	Terzaghi [129]; q_U (kPa)	Meyerhof [85]; q_U (kPa)	Hansen [39]; q_U (kPa)	Vesic [132]; q_U (kPa)	Present Experiment ; q_U (kPa) (Table 4.1)
Loose	15.79	35	37.2	64.4	52.5	46.6	65.0	58
Medium	16.23	70	38.3	81.4	66.3	57.8	80.0	91
Dense	16.70	90	39.0	95.2	77.5	66.9	92.0	128.3

γ – the unit weight of compaction; D_r - Relative Density of sand; φ_{tr} the internal angle of friction

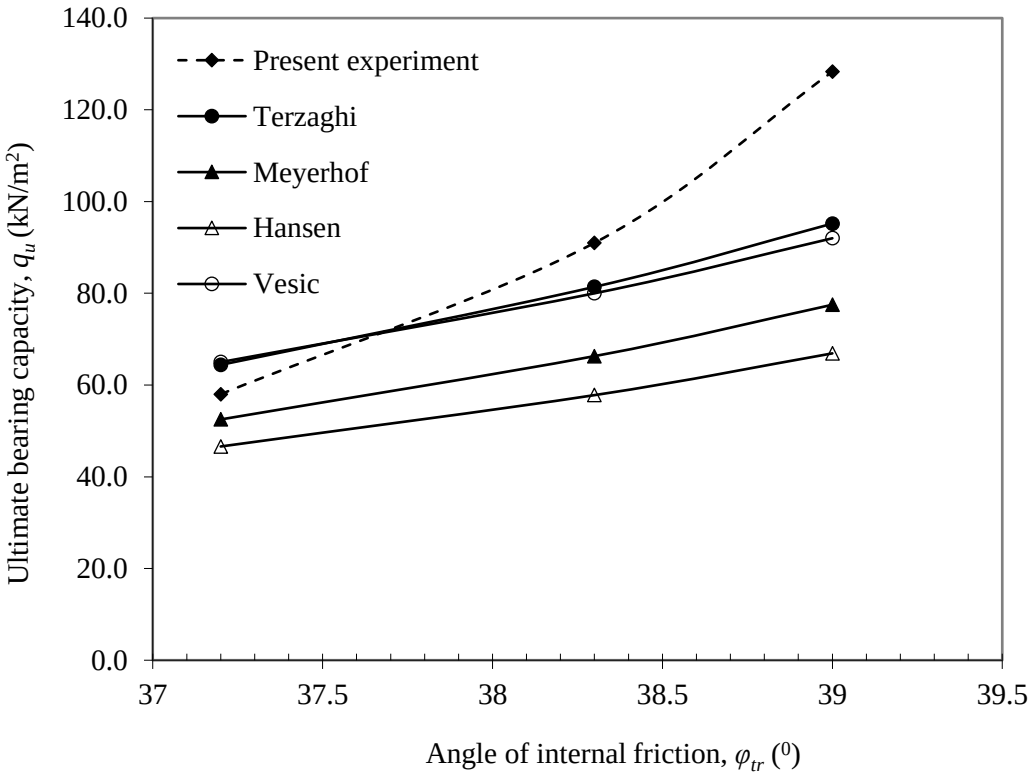

Fig. 4.10 Comparison of theoretical and experimental ultimate bearing capacity with an angle of internal friction for different states of sand.

The results in Fig. 4.10 indicate that there is a good agreement between the theoretical and experimental ultimate bearing capacity for loose and medium dense sand.

4.3 Geocell-reinforced sand beds

A series of model load tests (test series C1, D1, E1, F1, G1, H, and I, Table 3.4) are conducted to study the behavior of geocell-reinforced sand beds under static loading. The parameters varied are the shape of footing, geocell pocket size, the height of geocell, the width of geocell reinforcement, and relative density of subgrade sand & infill sand. In each test series, only one parameter is varied while the others are kept constant.

A typical pressure-settlement response for unreinforced and geocell-reinforced sand beds is depicted in Fig. 4.11(a-b). The performance improvements due to the provision of geocell-reinforced sand beds are quantified through two non-dimensional parameters-

(a) Bearing capacity improvement factor (*IF*): Improvement in bearing capacity of the footing which compares the bearing pressure of the geocell-reinforced sand (q_R) to that of the unreinforced sand at a given settlement level (q_U), as defined in eq. 4.8.

$$IF = q_{\mathrm{R}}/q_{\mathrm{U}} \tag{4.8}$$

(b) Percentage reduction of settlement (*PRS*): Improvement in footing settlement which compares the settlement of the geocell-reinforced bed (s_R) to that of the unreinforced bed (s_U) at the same level of bearing pressure, as defined below (eq. 4.6):

$$PRS = (1 - s_{\mathrm{R}}/s_{\mathrm{U}}\ ) \times 100 \tag{4.9}$$

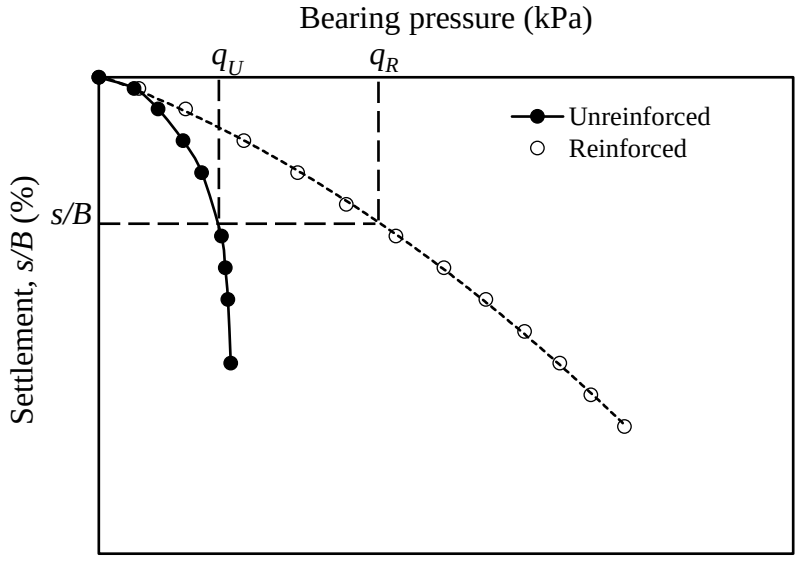

(a)

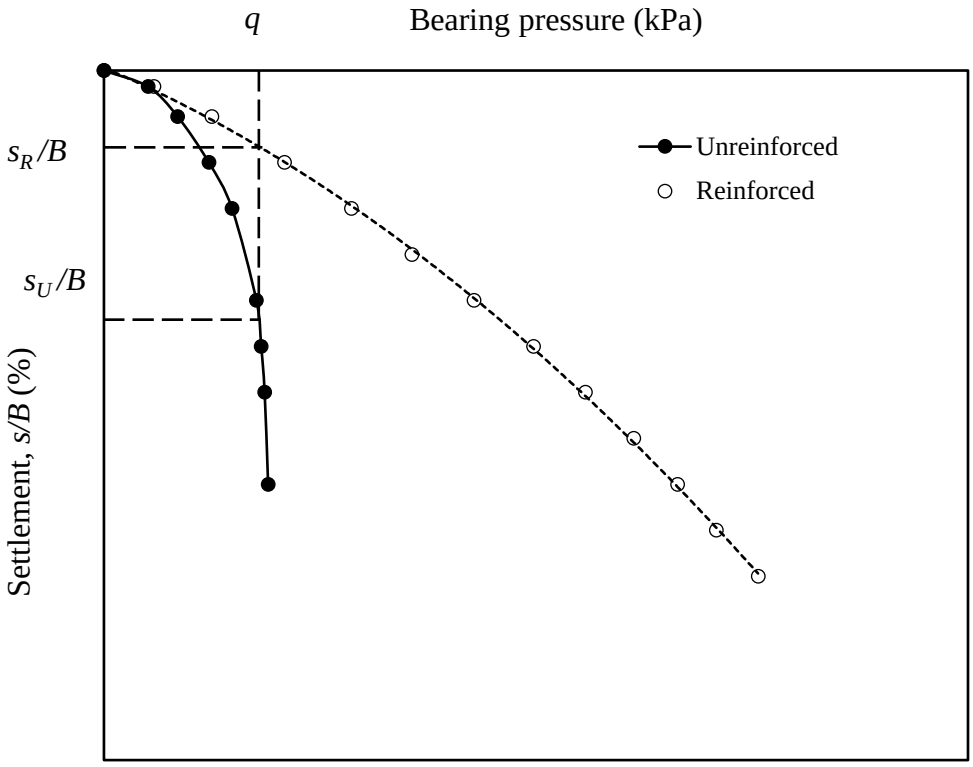

(b)

Fig. 4.11 Definition of parameters to determine improvements of geocell-reinforced sand in terms of (a) bearing capacity; (b) settlement

The influence of different geometric parameters such as pocket size, height and width of geocells, infill density of soil, and relative density of sand beds; on the overall response of the foundation system are presented and discussed in the following sections. The critical value of the geocell reinforcement and soil parameters are brought out by analyzing the test data based on the optimum performance improvement of the geocell-reinforced sand beds.

4.3.1 Effect of footing shape

In the test series I, the shape of the footings was varied as square, strip, and rectangular footings supported on reinforced sand with geocell with d/B = 0.5, h/B = 0.66, b/B = 3, u/B = 0.1 & D_r = 70%. Fig. 4.12 shows the relationship between the applied pressure and the normalized settlement for the three different types of footings supported on a geocell-reinforced sand bed.

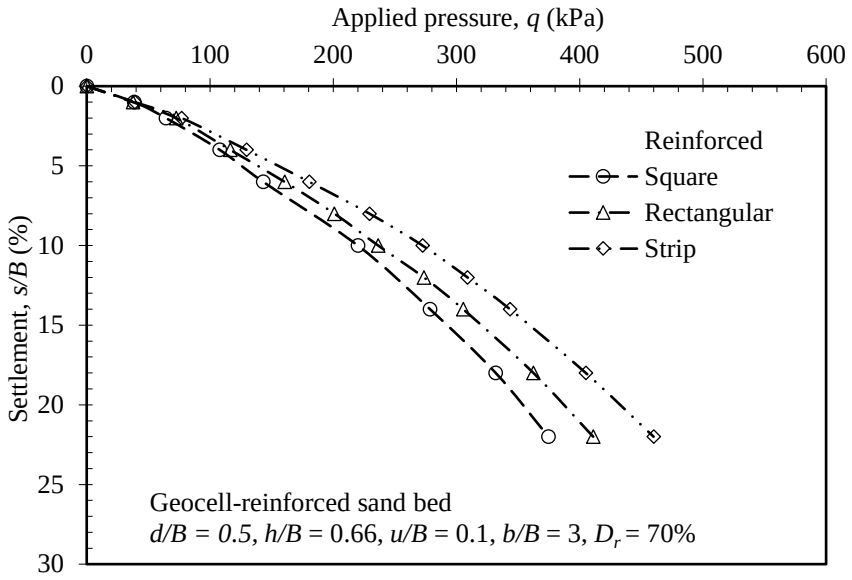

Fig. 4.12 Variation of footing settlement with load-bearing capacity for different types of footing supported on geocell-reinforced sand beds

The results illustrate no clear failure even up to a large settlement of s/B = 22%, as observed in unreinforced sand bed (Fig. 4.2). The results also reveal that at the normalized settlement of 10%, the load carrying capacity for strip footing is 272.5 kPa, whereas it is about 214 kPa and 236.5 kPa for square and rectangular footing, respectively.

The variation of improvement factor (*IF*) with footing settlements (*s/B)* for different types of footings is shown in Fig. 4.13.

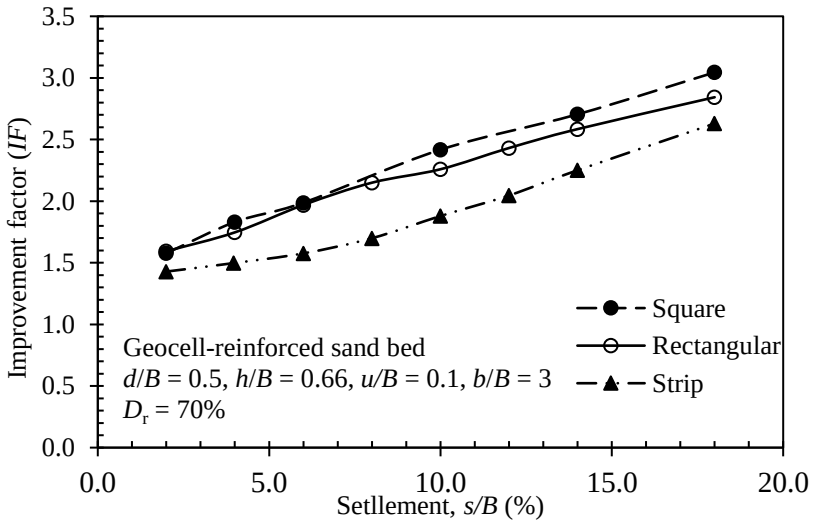

Fig. 4.13 Variation of Improvement factor (*IF*) with footing settlement for different shapes of footing supported on geocell-reinforced sand beds

The results show that *IF* increases as the ratio *B/L* increases from 0.0 (plane strain). This may be attributed due to the different ways of strain localization in the ground i.e. 3D failure mechanism of square and rectangular footings and 2D for the strip footing.

The surface deformation versus footing settlement plots, for different types of footings (square, rectangular, and strip footings) supported on geocell-reinforced sand beds are presented in Fig. 4.14a-c. Fig. 4.15 shows the variation of surface deformation at $x = 1.5B$ for geocell-reinforced sand beds of different types of footings. It can be seen from the figures that the surface heaving in comparison to unreinforced sand (Fig. 4.5a-c) has reduced around the footings with geocell reinforcement for all three types of footings. However, a small amount of surface heaving is observed at a distance $x = 1.5B$ due to the sagging deformation at the middle and hogging deformation at both ends of a relatively flexible geocell mattress (Fig. 4.15). Fig. 4.16 illustrates the amount of surface heaving at a distance $x = 1.5B$. It can be noted that the sagging and hogging deformation is more predominant at the larger settlement of footing only (i.e. beyond 10% of *s/B*).

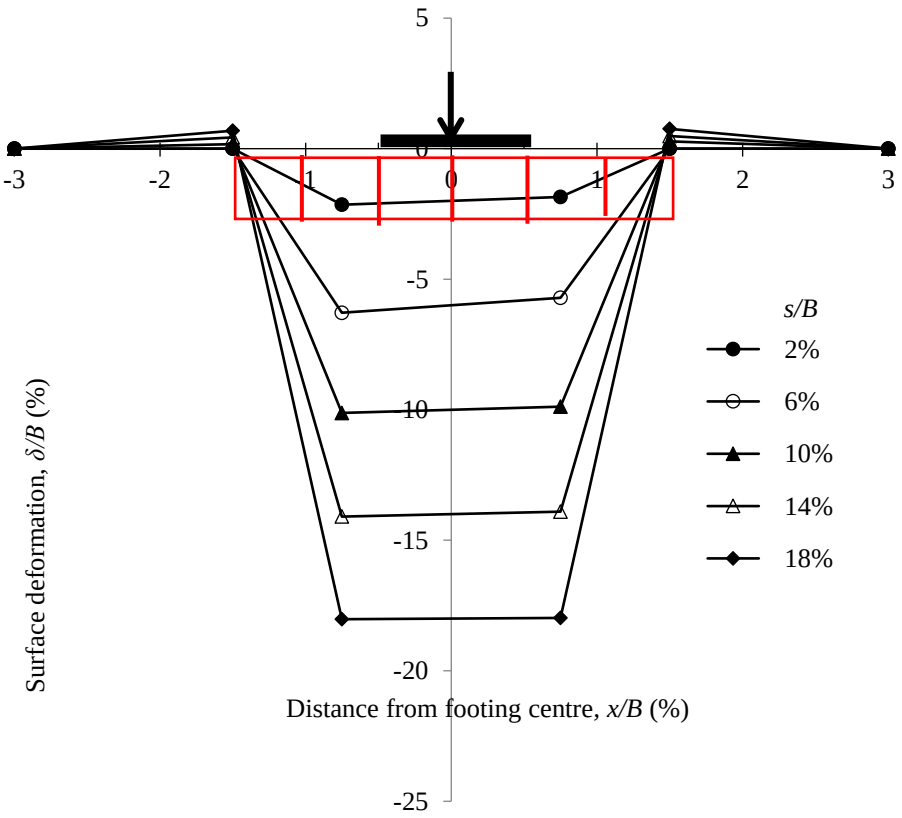

(a)

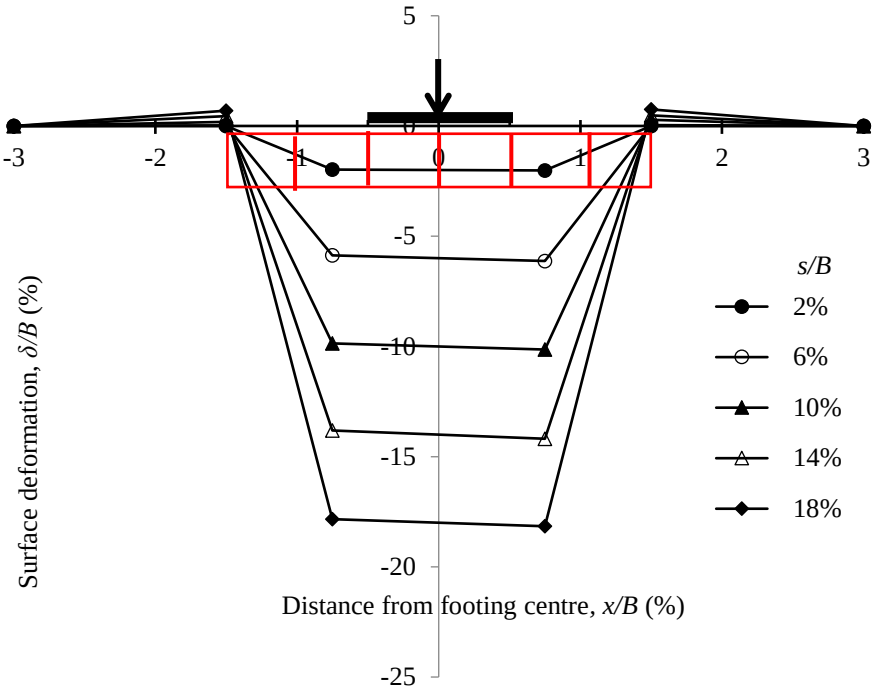

(b)

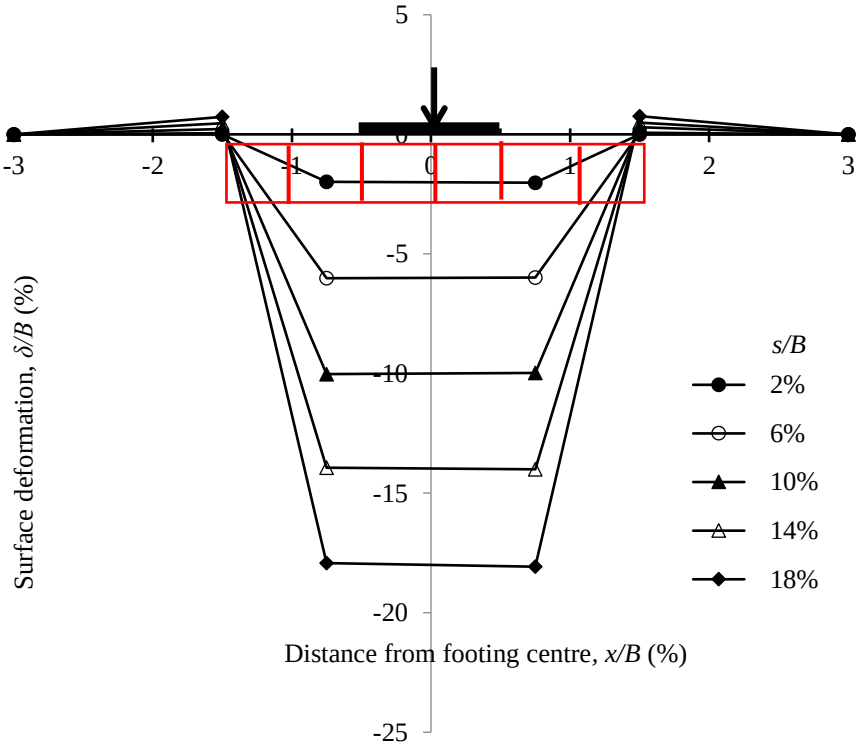

(c)

Fig. 4.14 Surface heaving with footing settlement for geocell-reinforced sand beds (D_r = 70%): (a) square footing; (b) rectangular footing; (c) strip footing.

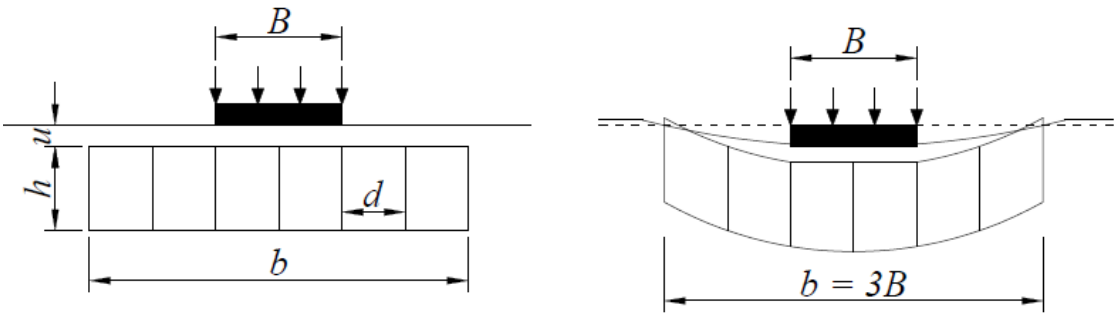

(a) (b)

Fig. 4.15 Schematic diagram of settlement and surface heaving of geocell-reinforced foundations system (a) before application of footing load, (b) after application of load footing load

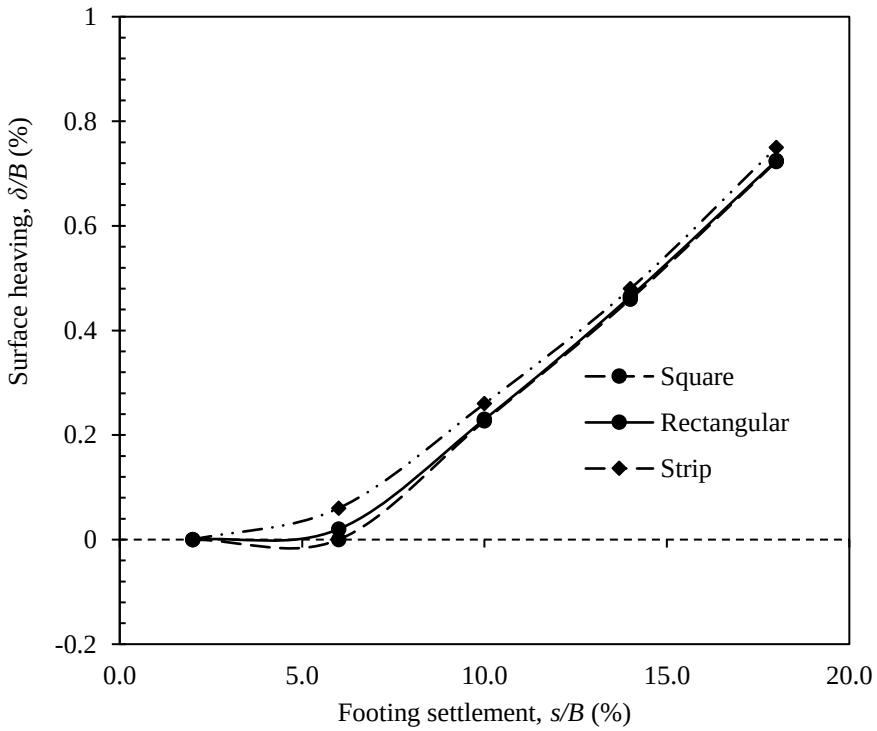

Fig. 4.16 Variation of surface deformations at $x = 1.5B$ for geocell-reinforced sand beds of different types of footings.

Since the performance improvement of square footing is observed to be better in comparison to rectangular and strip footing (Ref. Fig. 4.13 & Fig. 4.16), therefore, the geocell geometry and relative density of subgrade sand & infill sand that influences the performance of foundation is considered for square footing in the subsequent section of this study.

4.3.2 Effect of depth of geocell reinforcement position

The results were obtained from test series C1 as described in Table 3.4. The effect of the depth of geocell reinforcement position on the load-bearing capacity of geocell-reinforced sand (as compared to unreinforced sand) under square footing is presented in Fig. 4.17.

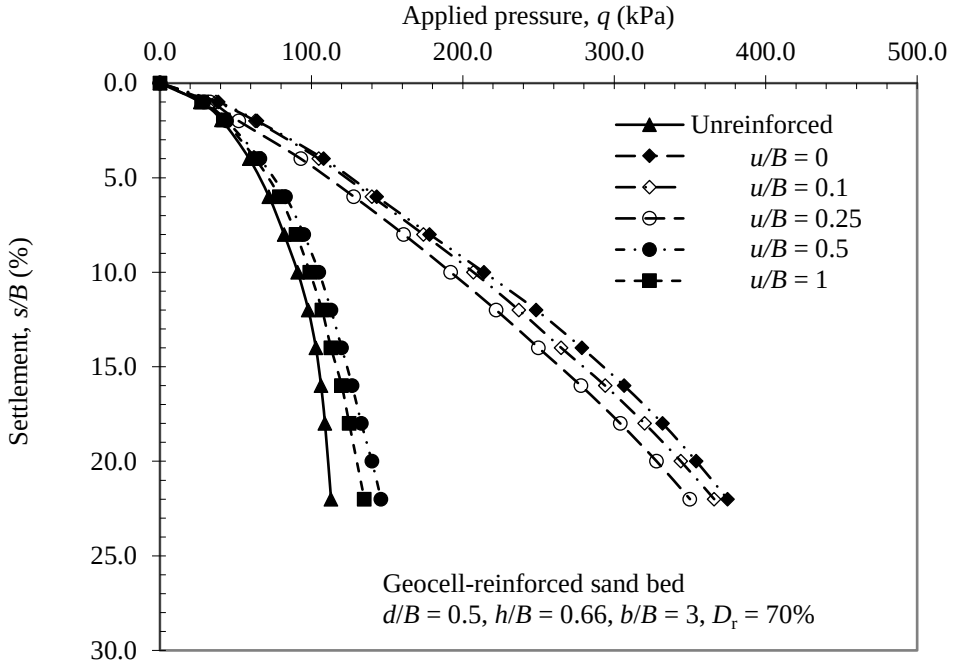

Fig. 4.17 Variation of footing settlement with load-bearing capacity for unreinforced and geocell-reinforced sand beds

The results show that the bearing capacity of the soil decreases as the depth of placement of the geocell layer increases up to $u/B = 0.5$, beyond which a very marginal increase in the load-carrying capacity of the reinforced soil is observed. The variation of *IF* with *u/B* at a different level of footing settlement is shown in Fig. 4.18. The results depict that the *IF* at the different levels of footing settlement generally decreases as the depth of placement of the reinforcement layer increases. Dash et al. [23], and Tafreshi and Dawson [123] have also reported the same observation when geocells made from geogrid and planar geotextile were used. This behaviour occurs because the location of the reinforcement layer is beyond the stress influence zone of the footing and the failure occurs between the base of the footing and the reinforcement layer; therefore, the membrane effect or confinement effect in the geosynthetic is not fully developed.

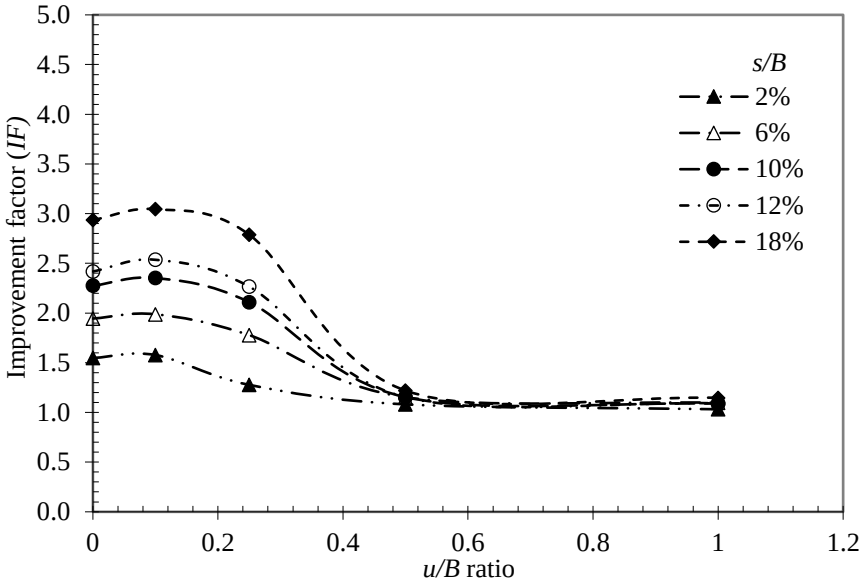

Fig. 4.18 Improvement Factor (*IF*) vs *u/B* ratio for different settlement

Fig. 4.19 illustrates the variation of percentage reduction of settlement (*PRS)* with different levels of footing settlement at different depths of placement of the geocell reinforcement layer. The figure indicates that *PRS* decreases with an increase in the depth of placement of the geocell layer from the top surface. The *PRS* was improved marginally when *u/B* increased from 0 to 0.1 and thereafter, the *PRS* value continue to decrease with an increase in the depth of placement. A similar marginal increase in *PRS* for near-surface placement of the geocell was also observed by Dash et al. [23].

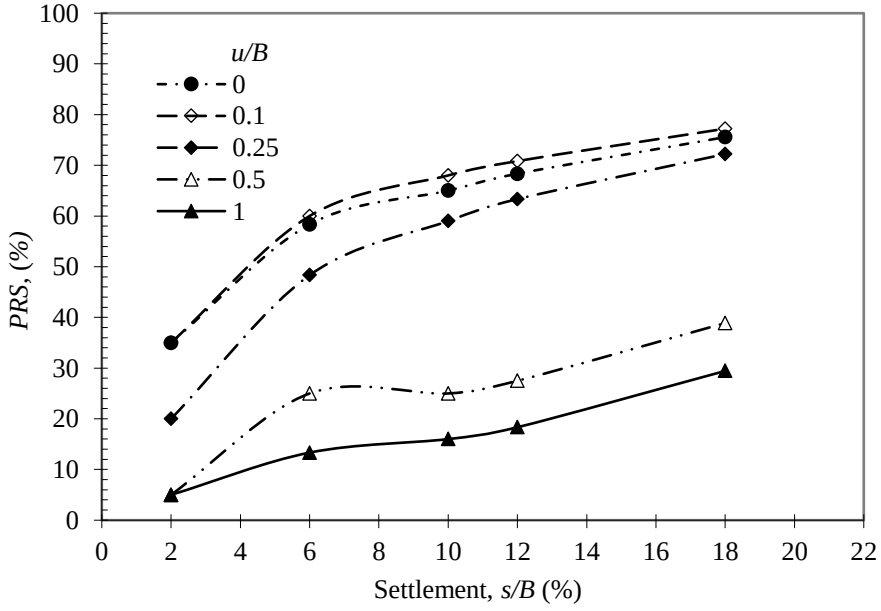

Fig. 4.19 Percentage reduction of settlement (*PRS*) vs *s/B* for different *u/B* ratio

The variation of average surface deformation with footing settlement for varied depths of placement of geocell reinforcement are presented in Figs. 4.20a-e. It could be observed that invariably for all cases (i.e. unreinforced and reinforced), the soil surface near the footing (i.e. $x = B$) settles at the initial stages of loading (i.e. $s/B < 10\%$). This is due to the dispersion of footing pressure over a wider area. Fig. 4.21 describes the amount of surface heaving at a distance $x = 1.5B$ from the centre of the footing for different depths of placement of the geocell layer from the base of the footing. With increased footing settlement, the soil fails and heaving takes place. It is also noted that for relatively shallow depths of placement (i.e. $u/B = 0$, 0.1 & 0.25), the settlement of the soil surface with geocell reinforcement is less compared to the corresponding unreinforced soil bed. However, when the depth of placement of the geocell reinforcement layer is increased beyond $0.5B$ (tested up to $1B$), settlement for both the unreinforced and reinforced foundation bed is almost the same indicating that at a larger depth of placement, the influence of geocell reinforcement is marginal. It can be seen that the surface heaving for the geocell layer placed at $u/B = 1$ and unreinforced sand is almost similar indicating the less influence of the geocell layer at that depth.

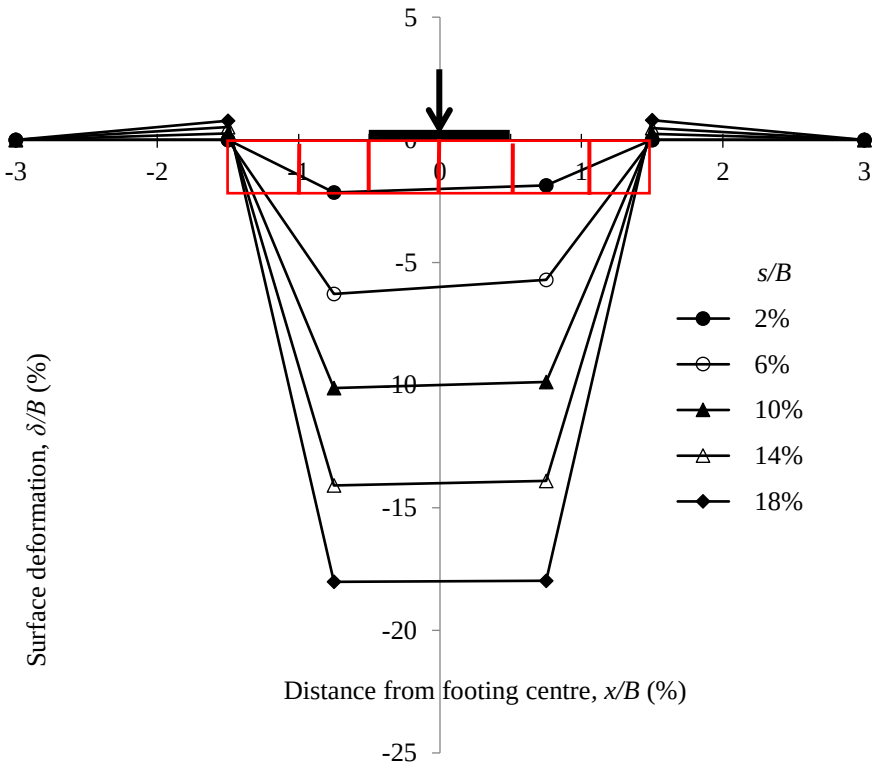

(a)

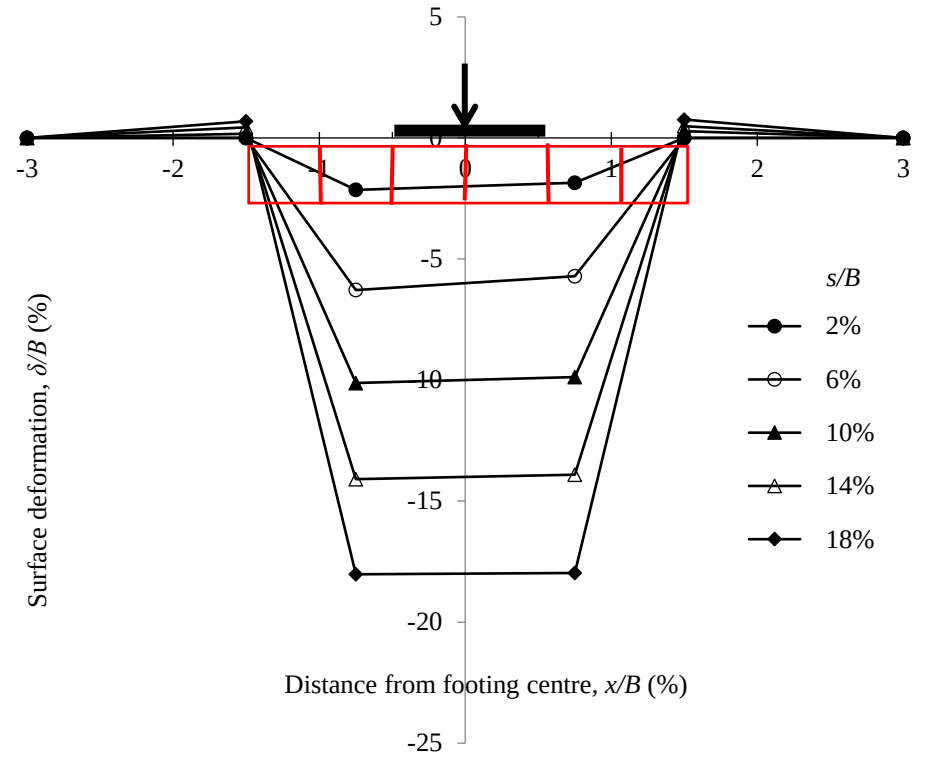
5
0
-5
-10
-15
-20
-25
-3
-2
-1
0
1
2
3
Surface deformation, δ/B (%)
Distance from footing centre, x/B (%)
s/B
2%
6%
10%
14%
18%

(b)

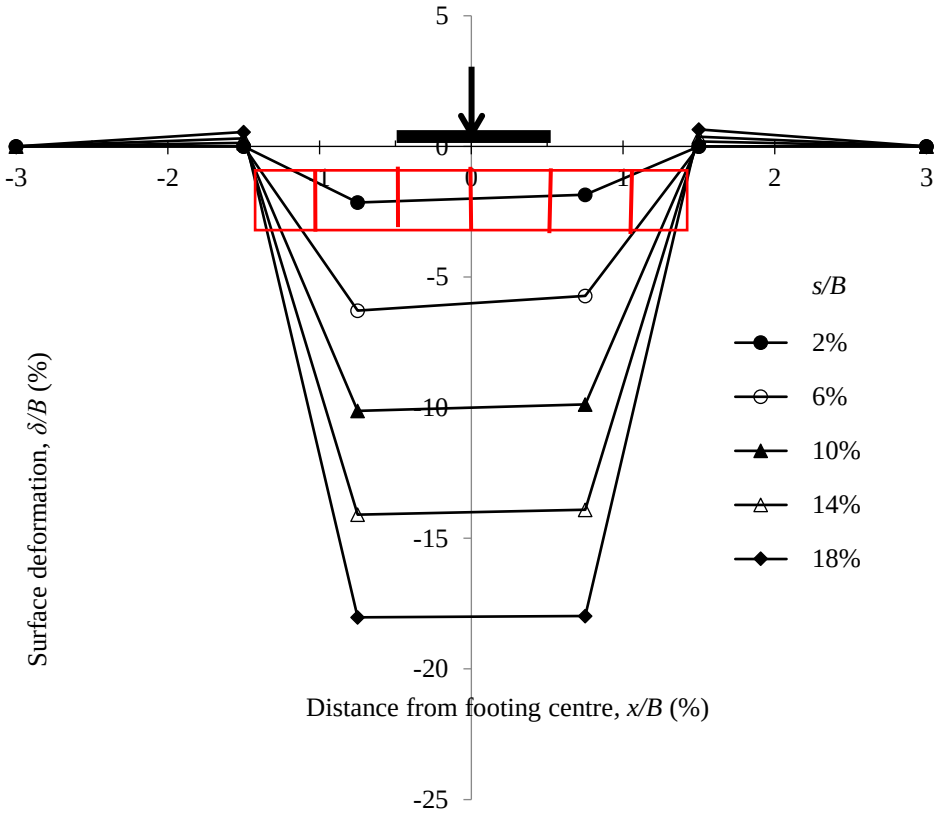
5
0
-5
-10
-15
-20
-25
-3
-2
-1
0
1
2
3
Surface deformation, δ/B (%)
Distance from footing centre, x/B (%)
s/B
2%
6%
10%
14%
18%

(c)

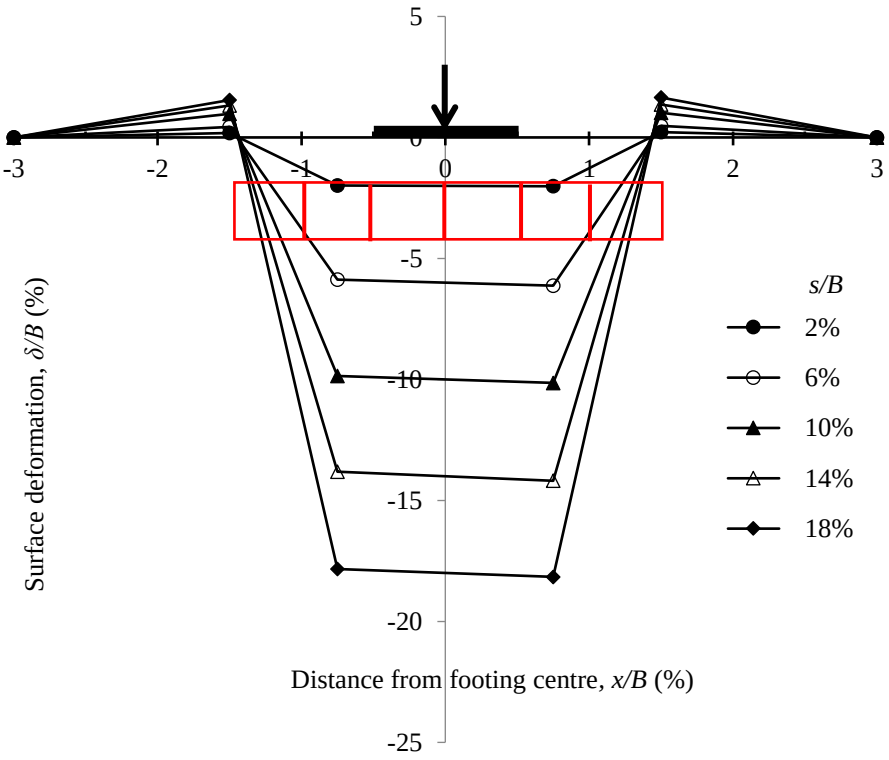

(d)

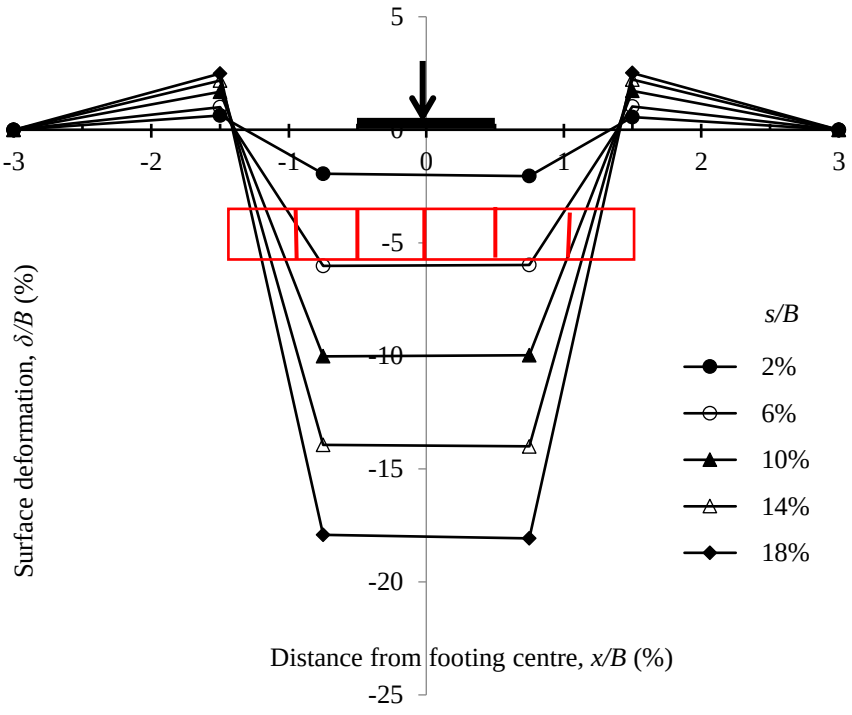

(e)

Fig. 4.20 Surface heaving with footing settlement for geocell-reinforced sand beds with geocell with d/B = 0.5, h/B = 0.66, b/B = 3, D_r = 70%: (a) u/B = 0; (b) u/B = 0.1; (c) u/B = 0.25; (d) u/B = 0.5; (e) u/B = 1.

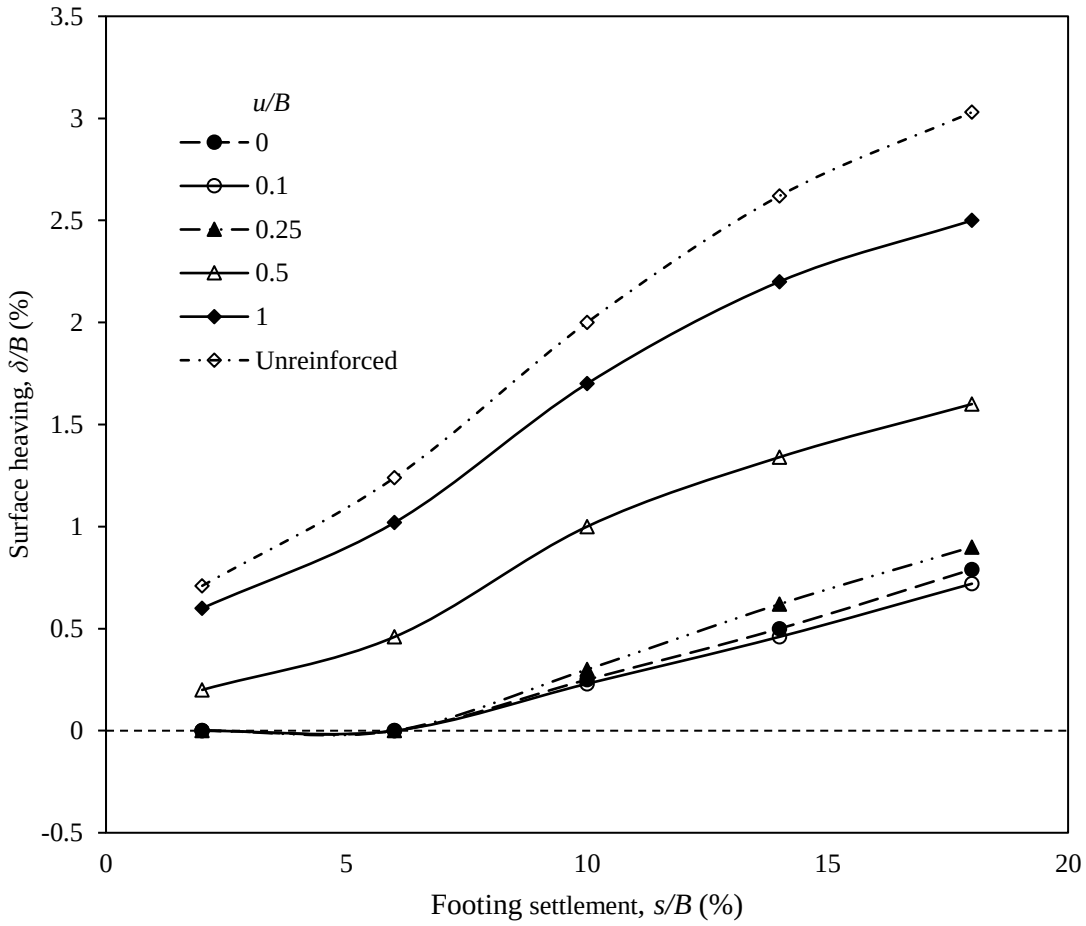

Fig. 4.21 Variation of surface deformations with footing settlement at a distance $x = 1.5B$ from the centre of footing, for different depths of placement (u) geocell reinforcement with geocell with $d/B = 0.5$, $h/B = 0.66$, $b/B = 3$, $D_r = 70\%$.

4.3.3 Effect of geocell pocket size

The bearing pressure versus settlement curves for different values of geocell pocket size ratio (d/B) is shown in Fig. 4.22, test series D1 (Table 3.4). It is observed that the rate of increase of bearing capacity of the soil starts to decrease for values of $d/B \geq 0.5$. For $d/B = 0.33$, the increase in bearing capacity is very marginal concerning that achieved with $d/B = 0.5$. This behaviour demonstrates that a sufficient pocket size must be provided to the geocell to fully develop the confinement, stress dispersion, and membrane effect in the reinforcement.

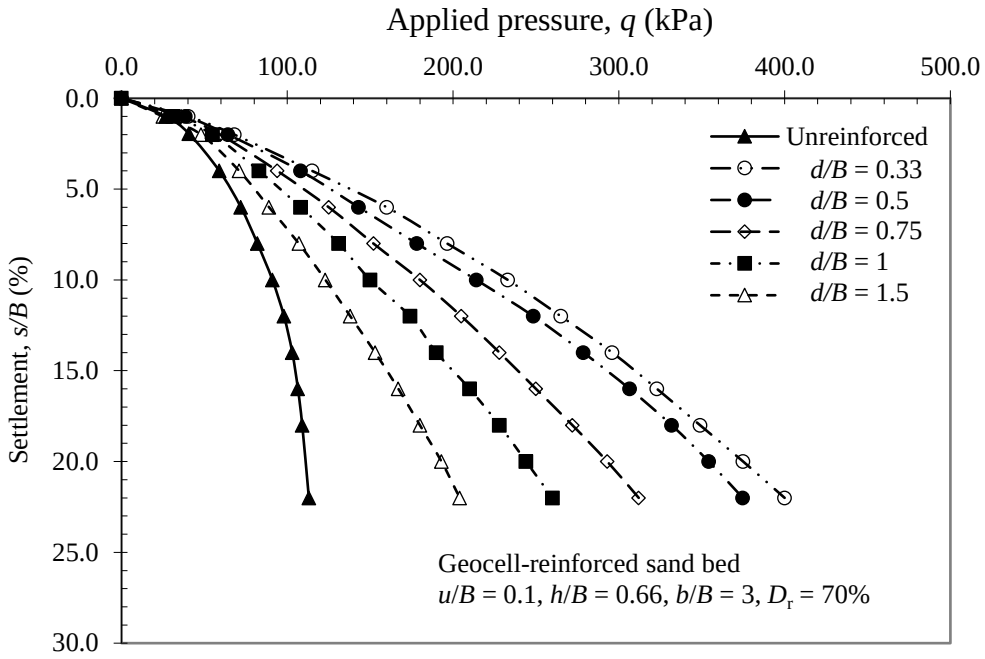

Fig. 4.22 Variation of footing settlement with bearing pressure for unreinforced and geocell-reinforced sand beds with different geocell pocket sizes.

Fig. 4.23 shows the variation of *IF* with the geocell pocket size ratio for different settlement levels. The *IF* decreases with increasing pocket size and the highest values of increase in the bearing capacity are reached for the pocket size ratio $d/B \leq 0.5$. The results also indicate a similar trend of behaviour for different settlement levels except at very low settlement, $s/B = 2\%$.

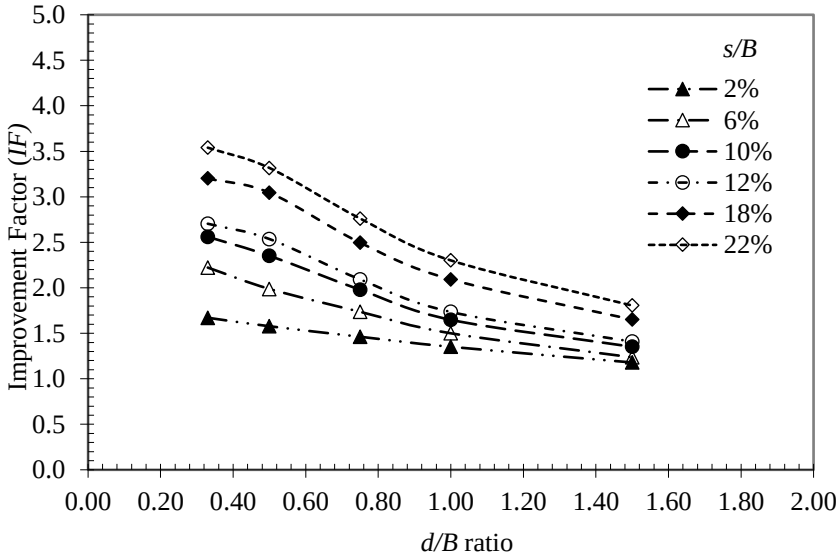

Fig. 4.23 Variation of bearing capacity improvement factor (*IF*) with footing settlement for the different pocket sizes of geocells

Fig. 4.24 depicts the effect of the size of the geocell pockets on the reduction of footing settlement at different settlement levels. It can be seen that *PRS* increases substantially at high ranges of footing settlement levels (> 6%). Besides, when the size of the geocell pocket is 0.33 (*d/B*), the influence of geocell reinforcement on the reduction of footing settlement is 70% at the measured settlement level *s/B* = 10%. However, when the size of the geocell pocket is 1.5 (*d/B*), the geocell reinforcement only results in a 38% reduction in footing settlement. This indicates that for better performance of geocell reinforcement under the footing, the size of the geocell pocket should preferably be not larger than the footing width.

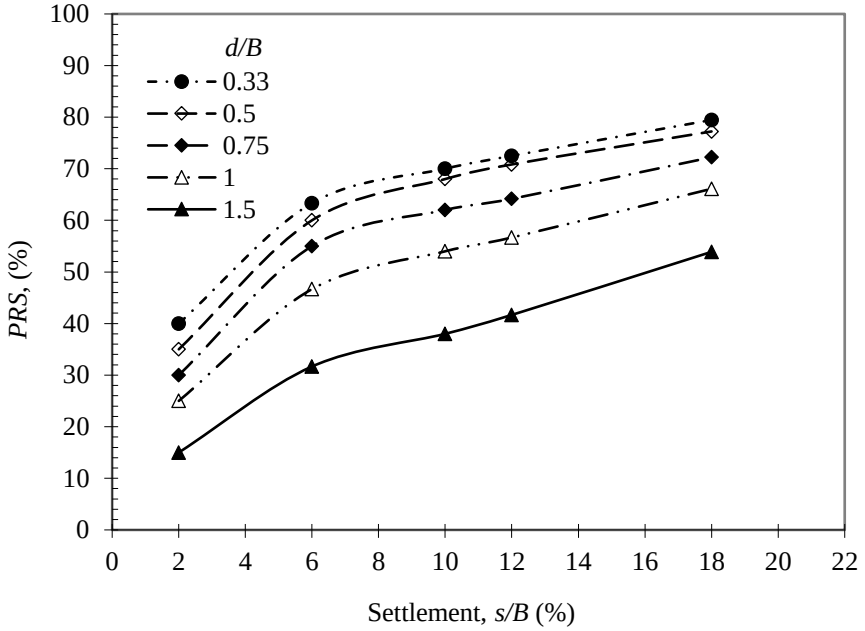

Fig. 4.24 Variation of *PRS* versus footing settlement for different geocell pocket sizes.

Fig. 4.25(a-e) depicts the surface deformation versus footing settlement responses for pocket sizes varying from 1.5 to 0.33*B*. Fig. 4.26 shows the surface deformations with footing settlement at a distance $x = 1.5B$ from the centre of footing, for different pocket sizes (d) of geocell reinforcement. It could be seen that for $d = 1.5B$ (Fig. 4.26), the responses of unreinforced and reinforced soil are nearly similar till settlement of about 5-10% of B indicating that over this settlement range, the influence of reinforcement is marginal. Further, this also indicates that the improvement due to geocell reinforcement of large pocket size is manifested only at higher settlements. However, with the reduced pocket sizes of geocells (d = 1B, 0.75B, 0.5B, and 0.33B), the influence of the

reinforcement is observed at much lower settlement (Figs. 4.25a to 4.25e). These observations indicate that for geocells of very large pocket size (d = 1.5B), the deformed sand under the footing passes down almost unhindered through the large openings of the geocell pockets which indicates that the geocell reinforcement plays only a marginal role. It is only at very large deformation that the reinforcing effect is manifested possibly through some indirect actions such as mobilization of anchorage and passive resistance from the soil in the region outside the loading area. While with reduced pocket size, the relatively closer geocell structure effectively restrains the downward moving soil mass, under footing penetration, leading to the manifestation of reinforcing action at much earlier stages of settlement.

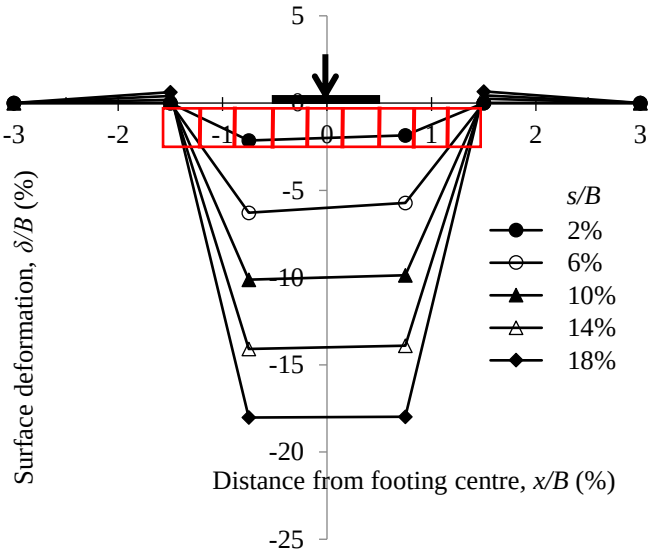

(a)

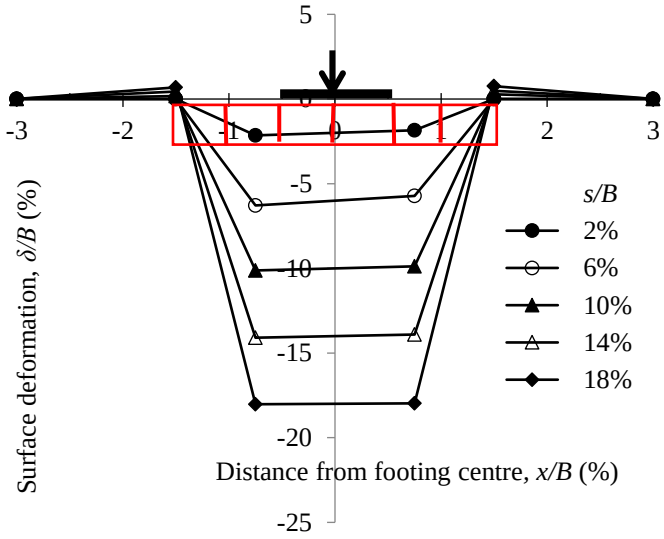

(b)

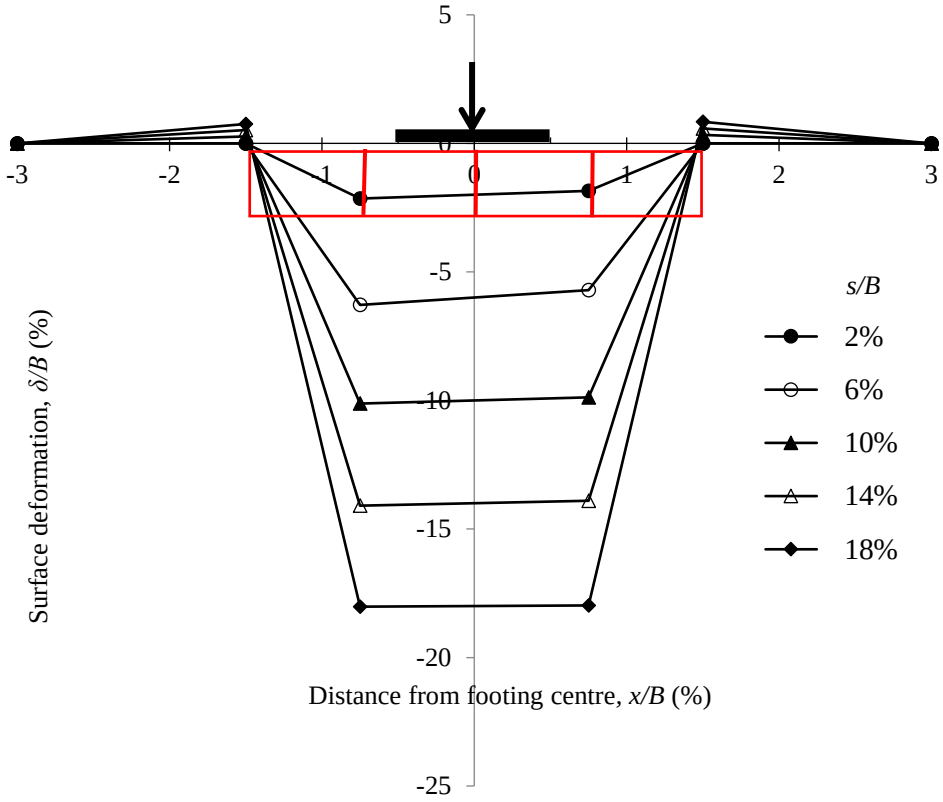
5
0
-5
-10
-15
-20
-25
-3
-2
-1
0
1
2
3
Surface deformation, δ/B (%)
Distance from footing centre, x/B (%)
s/B
2%
6%
10%
14%
18%

(c)

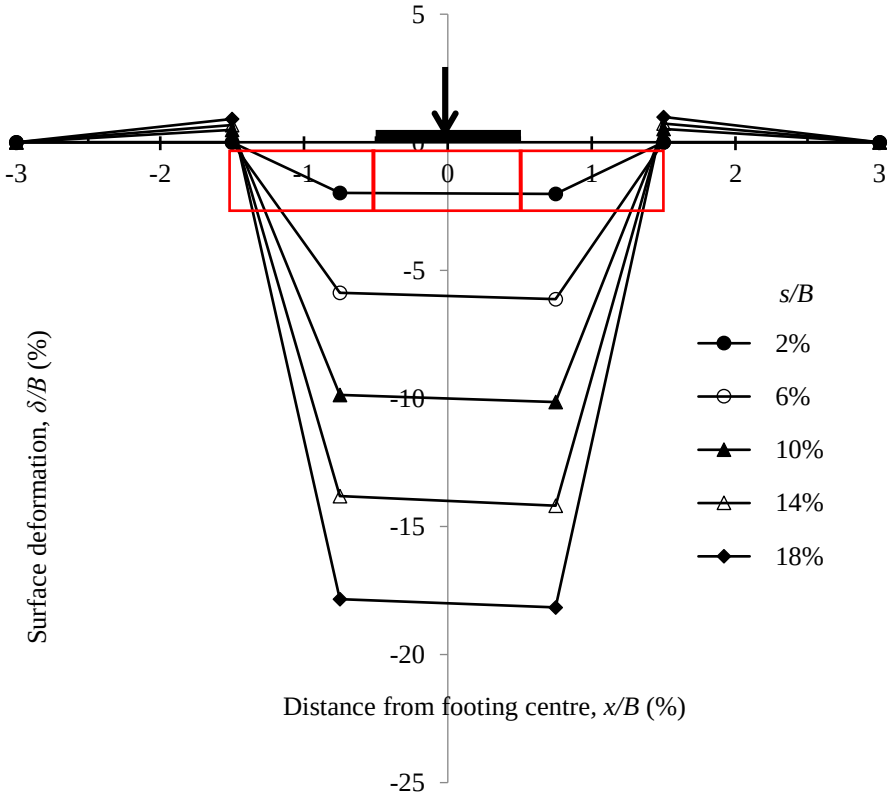
5
0
-5
-10
-15
-20
-25
-3
-2
-1
0
1
2
3
Surface deformation, δ/B (%)
Distance from footing centre, x/B (%)
s/B
2%
6%
10%
14%
18%

(d)

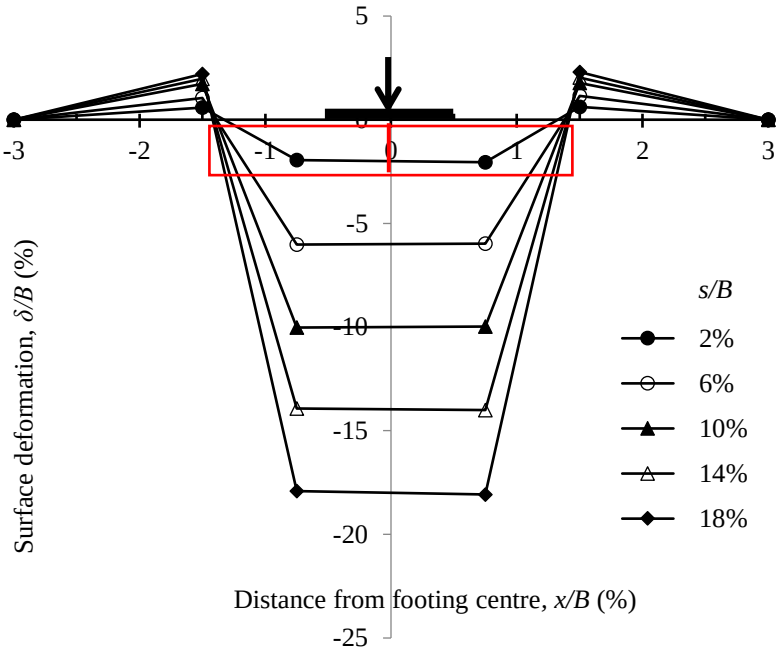

(e)

Fig. 4.25 Surface heaving with footing settlement for geocell-reinforced sand beds with geocell with u/B = 0.1, h/B = 0.66, b/B = 3, D_r = 70%, (a) d/B = 0.33; (b) d/B = 0.5; (c) d/B = 0.75; (d) d/B = 1; (e) d/B = 1.5.

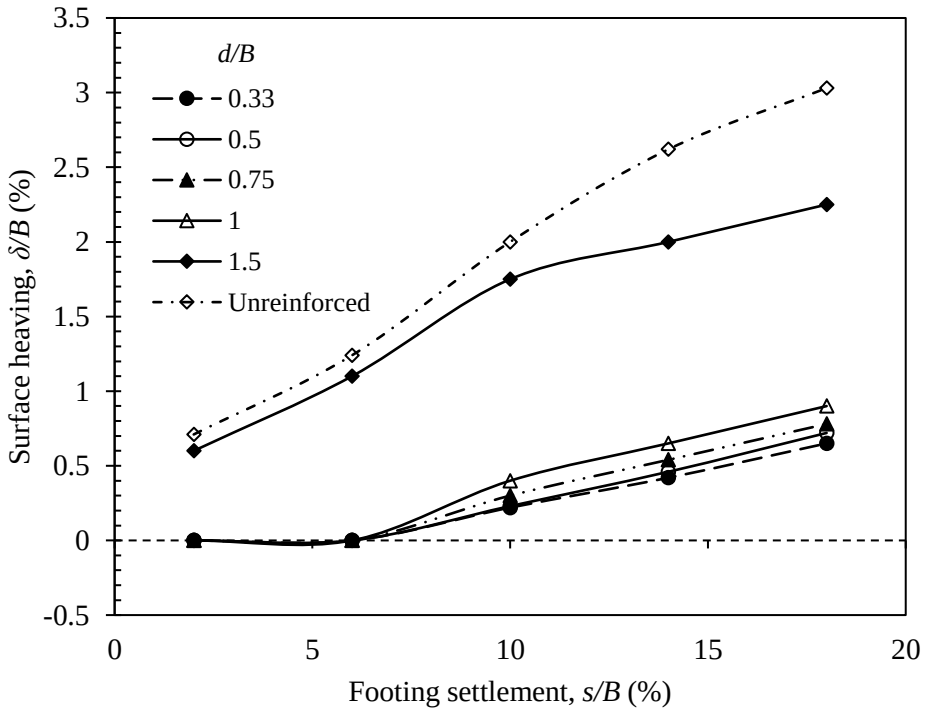

Fig. 4.26 Variation of surface deformations with footing settlement at a distance x = 1.5B from the centre of footing, for different pocket sizes (d) of geocell reinforcement with geocell with u/B = 0.1, h/B = 0.66, b/B = 3, D_r = 70%.

4.3.4 Effect of height of geocell mattress

In general use of geocell reinforcement significantly enhances the bearing capacity of the footing in comparison to unreinforced soil. Test series E1 (Table 3.4) was conducted to investigate the effect of the height of the geocell mattress on the ultimate bearing capacity of geocell-reinforced sand beds. Fig. 4.27 shows the pressure-settlement behaviour of footing supported on unreinforced and geocell-reinforced sand with different geocell heights. It is noticed that an increase in height of geocell reinforcement increases the bearing capacity and stiffness of reinforced sand. This is because of increase in height of geocell reinforcement increases the overall frictional resistance due to the increase in surface area and as a result the resistance to the downward movement of the soil increases. An increase in bending rigidity of geocell as a result of an increase in height and consequent redistribution of footing pressure over a wider area was also noted as a cause of performance enhancement of the reinforced soil by Dash et al. [23], Kargar and Hosseini [60].

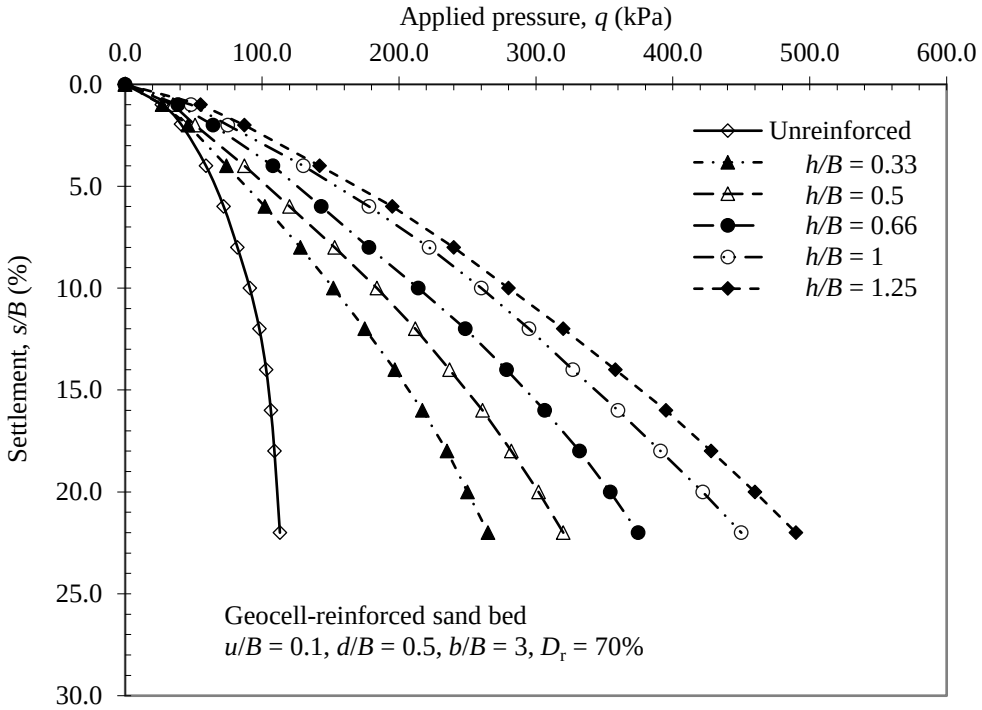

Fig. 4.27 Variation of footing settlement with bearing pressure for different heights of geocell mattress

Fig. 4.28 represents the variation of bearing capacity improvement factor (*IF*) with geocell height ratio at different footing settlement levels. The results indicate that *IF* initially increases with a greater gradient (up to *h/B* = 0.66) and thereafter, it increases with a gentle gradient indicating the optimum level of cell height. It is also observed that as the height of the geocell layer increases from *h/B* = 0.33 to *h/B* = 1.25, the *IF* increases from 1.7 to 3.1 at the measured footing settlement level *s/B* = 10%. Besides, *IF* of 1.1 to 2.1 is observed for *h/B* = 0.33 to 1.25 at measured settlement level *s/B* = 2%, illustrating the influence of geocell height on bearing capacity even at low levels of footing settlements.

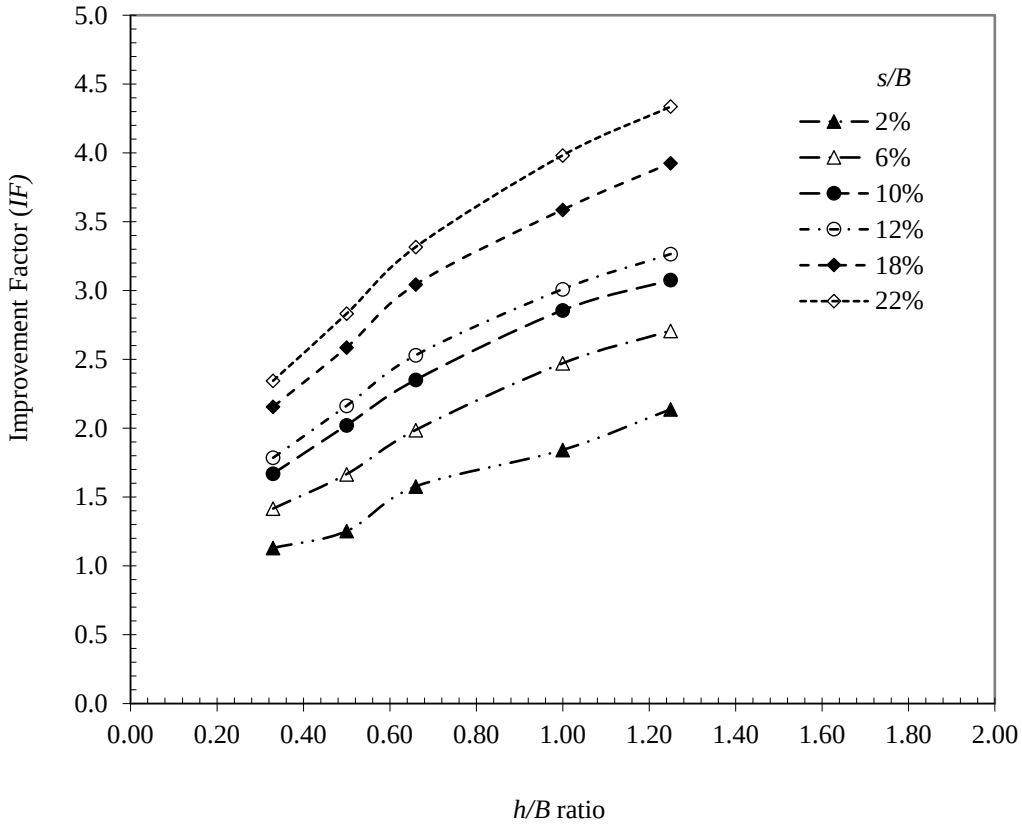

Fig. 4.28 Variation of bearing capacity *IF* with *h/B* ratio at different settlement levels

The plot between *PRS* versus settlement for different geocell heights is shown in Fig. 4.29. The test result implies that *PRS* value increases with an increase in settlement level for different geocell height ratios. The *PRS* increases steeply from settlement level 2% to 10% of *B*, and thereafter, it increases marginally (*s/B* = 10% to 22%). This behaviour may be due to the fact that unreinforced soil fails at a settlement level of about 6-10% of footing width, and hence, the complete participation of reinforcement takes place at this range of

settlement. The *PRS* for geocell height ratio 0.66 (*h/B*) was observed at about 35%, 68%, and 80.5% at the measured settlement level, 2%, 10% & 18% (*s/B*), respectively.

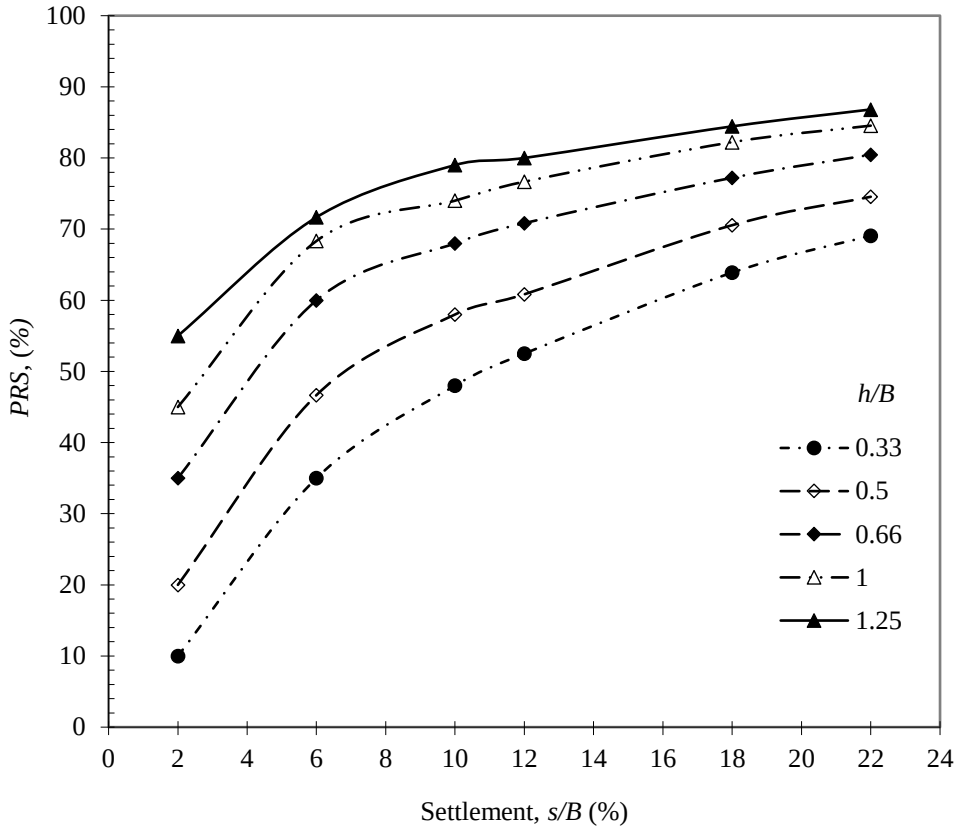

Fig. 4.29 Variation of *PRS* versus footing settlement for different heights of geocell mattress

The surface deformation versus footing settlement responses at distances of $x = B$, $1.5B$, and $3B$ from the centre of the footing, for a geocell mattress of height, $h = 0.33B$, $0.5B$, $0.66B$, $1B$, and $1.25B$ are shown in Figs. 4.30(a-e). Fig. 4.31 demonstrates the surface deformations with footing settlement at a distance $x = 1.5B$ from the centre of footing, for different heights (h) of geocell reinforcement. It can be seen that with increases in geocell mattress height, surface heaving decreases. Besides, the prominent heaving on the soil surface which is observed in $h = 0.33B$, $0.5B$, and $0.66B$, at $x = 1.5B$ (Fig. 4.31), is absent in the case of higher height of geocell layer ($h = 1B$ and $1.25B$). This may be because the geocell mattress of low height being flexible undergoes a sagging type of deformation under the loading and correspondingly hogging type of deformation in the region outside thereby giving rise to an induced heaving at $x = 1.5B$. Whereas, the geocell mattress of

higher height behaves as a relatively rigid pad that settles in a much uniform manner leading to reduced heave on the soil surface. Further, the increased height of geocell reinforcement offers better confinement of the infill material thus leading to lesser heave.

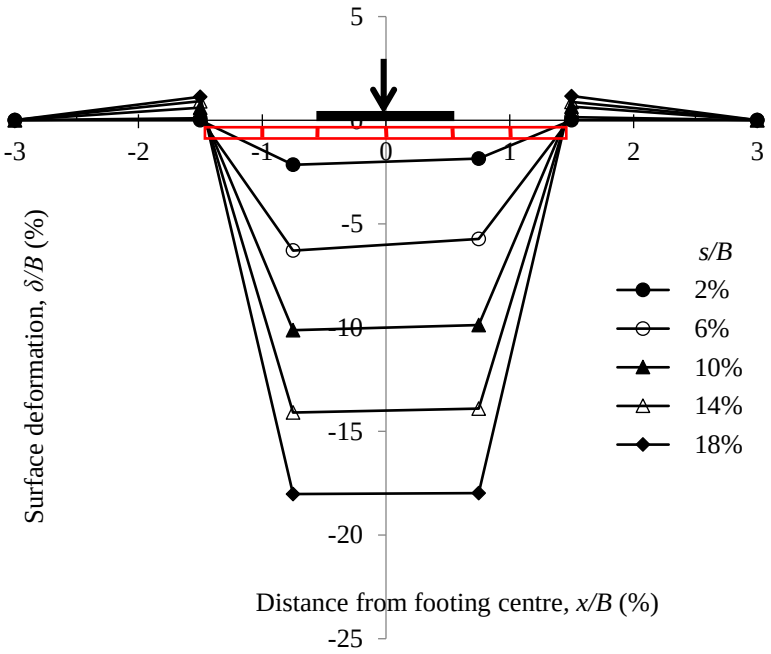

(a)

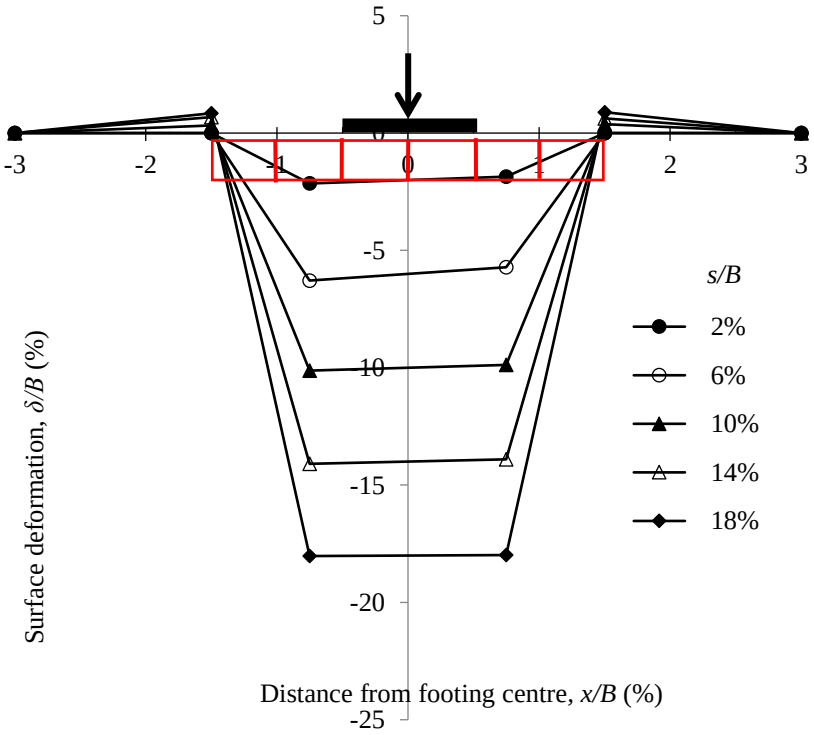

(b)

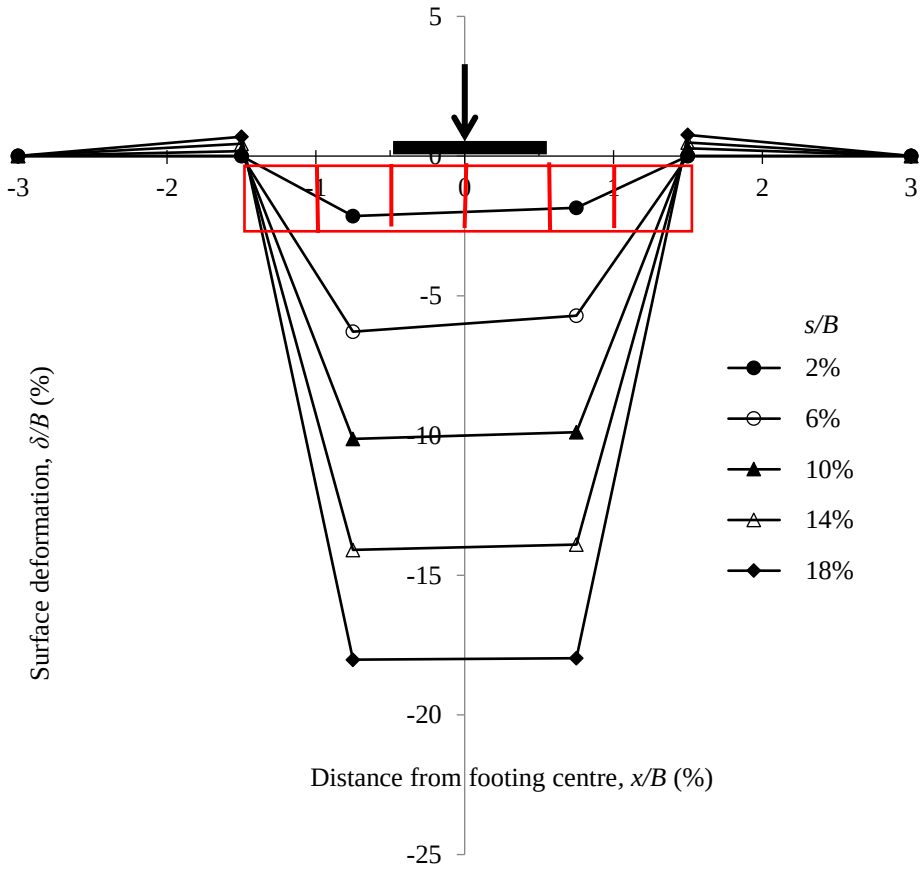
5
0
-3
-2
-1
0
1
2
3
-5
-10
-15
-20
-25
Surface deformation, δ/B (%)
Distance from footing centre, x/B (%)
s/B
2%
6%
10%
14%
18%

(c)

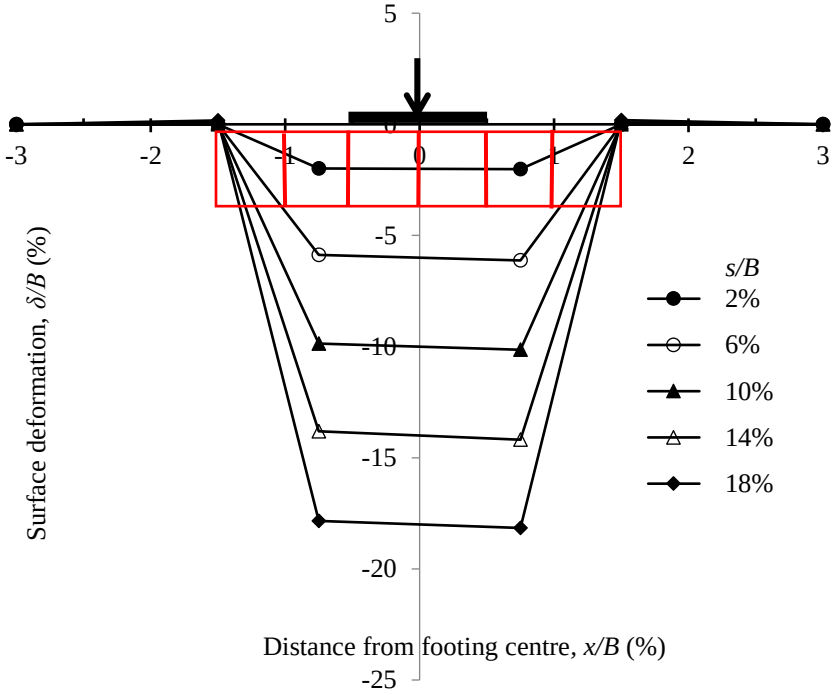
5
0
-3
-2
-1
0
1
2
3
-5
-10
-15
-20
-25
Surface deformation, δ/B (%)
Distance from footing centre, x/B (%)
s/B
2%
6%
10%
14%
18%

(d)

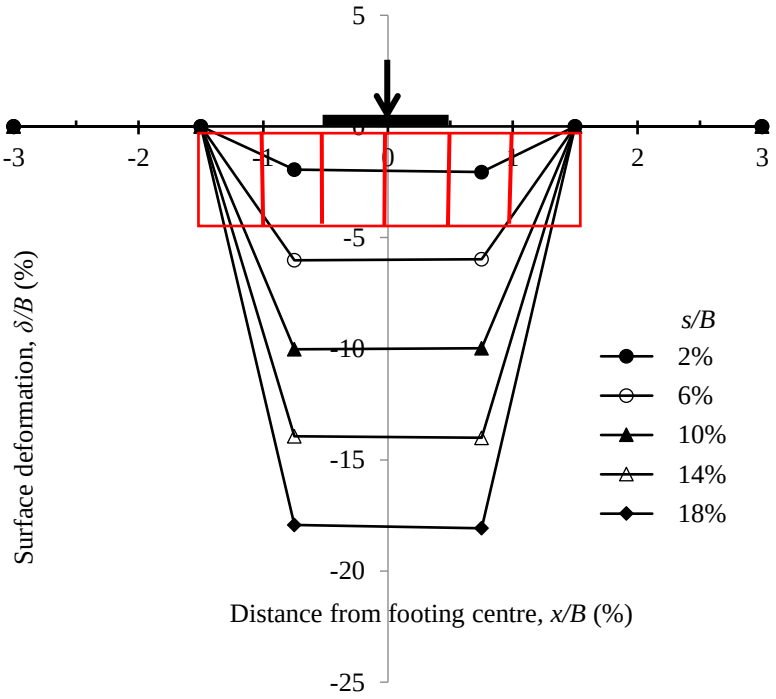

(e)

Fig. 4.30 Surface heaving with footing settlement for geocell-reinforced sand beds with geocell with d/B = 0.5, u/B = 0.1, b/B = 3, D_r = 70%, (a) h/B = 0.33; (b) h/B = 0.5; (c) h/B = 0.66; (d) h/B = 1; (e) h/B = 1.25.

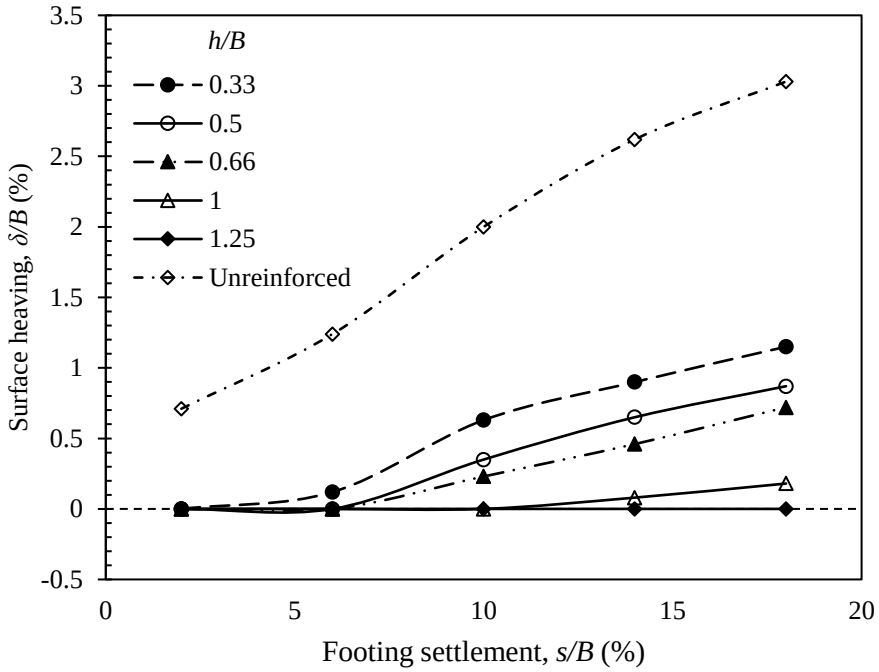

Fig. 4.31 Variation of surface deformations with footing settlement at a distance x = 1.5B from the centre of footing, for different height (h) of geocell reinforcement with geocell with u/B = 0.1, d/B = 0.5, b/B = 3, D_r = 70%.

4.3.5 Effect of geocell-reinforcement width

Fig. 4.32 illustrates the effect of geocell reinforcement width on the load-settlement behavior of geocell-reinforced sand bed with 70% relative density, test series F1 (Table 3.4). Fig. 4.33 shows the influence of geocell reinforcement width on the bearing capacity improvement factor for different settlement levels of footing. The test data reveals that the performance of the geocell-reinforced foundation system, both in terms of bearing capacity and settlement, increases with an increase in geocell reinforcement width. For instance, the bearing capacity Improvement Factor is about 2.1 and 2.5 for reinforcement width, $b = 2B$ and $b = 3B$, respectively, at $s/B = 12\%$, $D_r = 70\%$. However, the effect of improvements diminishes when the width of the geocell reaches its optimal value of $3B$, as depicted in Fig. 4.33.

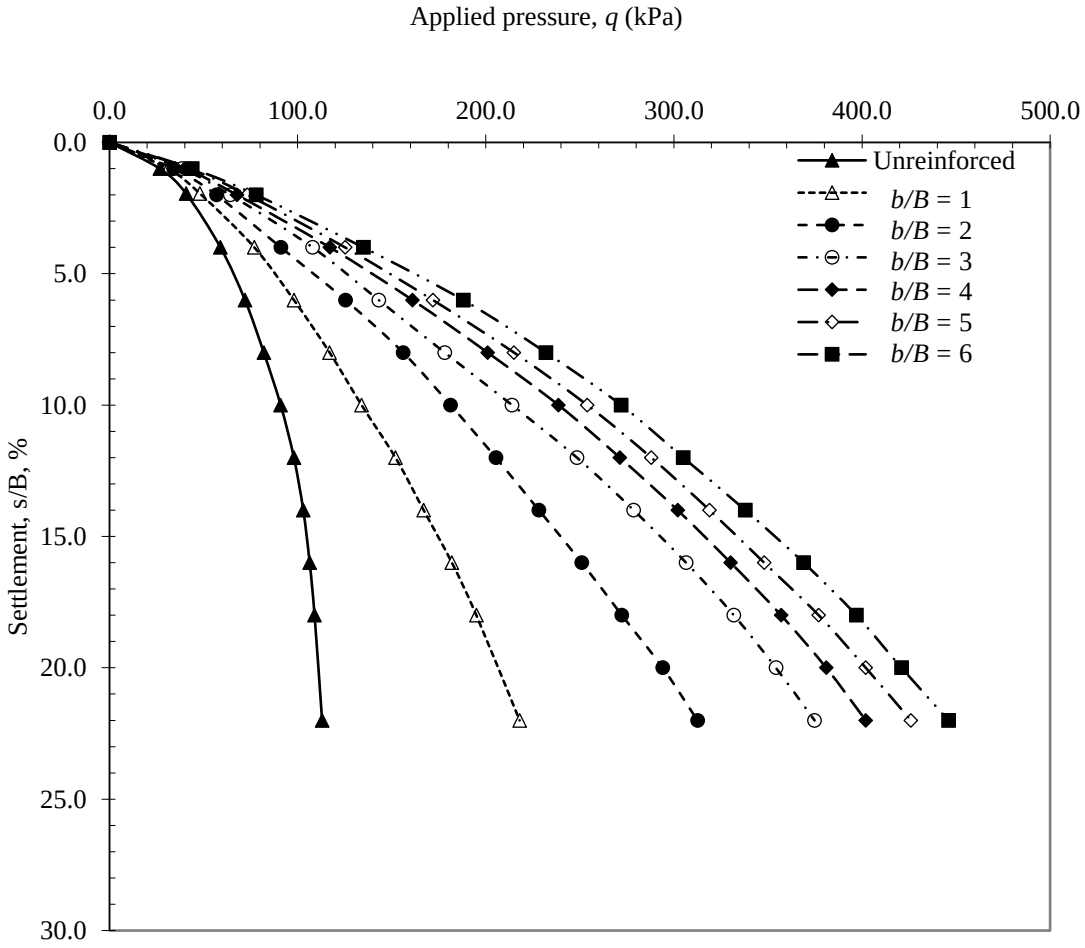

Fig. 4.32 Variation of footing settlement with bearing pressure for different widths of geocell reinforcement

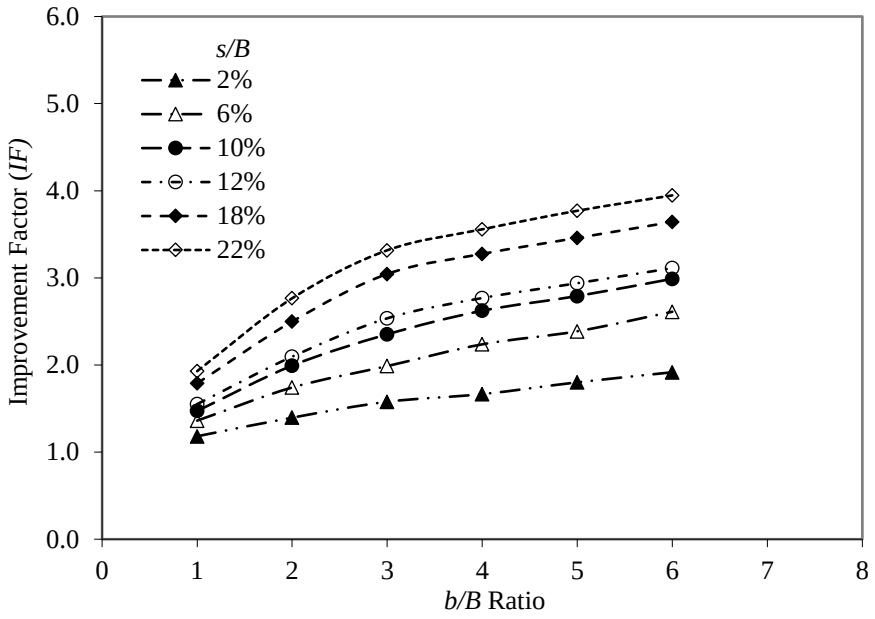

Fig. 4.33 Improvement Factor vs *b/B* ratio for different settlement level

It may be noted that an increase in the geocell width ratio from 1 to 3 (*b/B*) significantly increases *IF* from 1.6 to 2.4 at *s/B* = 10%. This can be attributed to the fact that by increasing the width of geocell reinforcement on both sides of the footing the interception of failure planes in the geocell-reinforced foundation system increases. However, a further increase in reinforcement width (> *b*/*B* = 3) shows a marginal enhancement in the ultimate bearing capacity of the footing.

It is noteworthy that despite the limited ability of the geocell mattress to control failure planes in the case of a short-width geocell reinforcement equal to the footing width, the Improvement factor (*IF*) still increased by 1.6 compared to unreinforced soil. This is because the geocell mattress serves as a rigid cushion, transferring the load from the footing to the base of the geocell, which acts like a deeply embedded footing.

The variation of percentage reduction in settlement (*PRS*) versus footing settlement for different widths of geocell reinforcement is shown in Fig. 4.34. It can be seen that the gradient of the curve of *PRS* is very steep at settlement ranges of *s/B* ≤ 6%. However, for higher settlement ranges (*s/B* ≥ 6%), soil reinforcement increases the value of *PRS* with gentle slopes which implies that the internal confinement, provided by geocell inclusion, increases with an increase in the imposed settlement level on the reinforced system after failure point of unreinforced soil (beyond *s/B* = 6%).

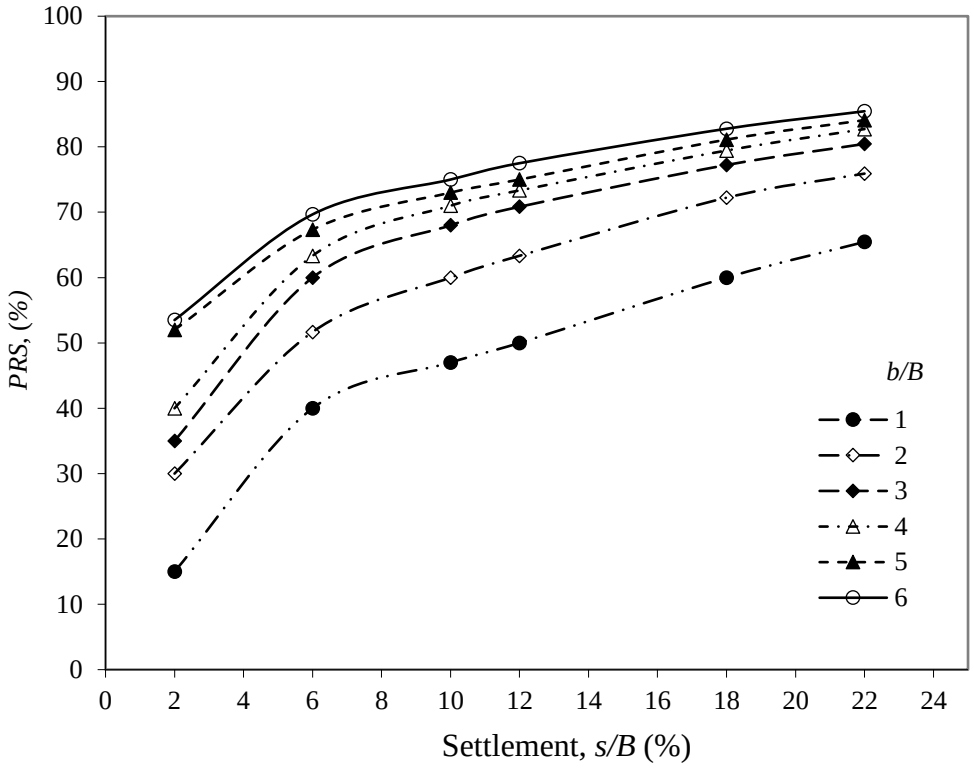

Fig. 4.34 *PRS* versus footing settlement for different reinforcement width ratio

Fig. 4.35(a-e) represents the surface deformation profiles for different widths of the geocell reinforcement layer at different *s/B* ratios. The progression of the settlement or heaving for each increment can be tracked using the figures. It can be seen that the use of geocell reinforcement almost arrests the surface heaving of soil irrespective of which width of reinforcement layer has been used. However, the magnitude of surface heaving decreases with the increases in the width of the reinforcement layer. This may be attributed to the increase in stiffness of the foundation system due to the introduction of the reinforcement layer. Fig. 4.36 shows the variation of surface heaving at $x = 1.5B$ from the centre of the footing, for different widths of geocell reinforcement. It can be observed from the figure that positive surface heaving has taken place for reinforcement layer widths 1*B* to *3B*. This may be because to measure the surface heaving dial gauges are placed at $x = 1.5B$ which is outside or at the edge of the geocell reinforcement layer in case of smaller width ($b = 1B$ to $3B$). Thus, sagging and hogging deformation has taken place at the centre and outside the loading area of the footing simultaneously. However, as the width of the reinforcement layer increases beyond $b = 4B$, negative surface heaving ($-\delta/B$ %) has taken place due to sagging deformation near the loaded area of the footing.

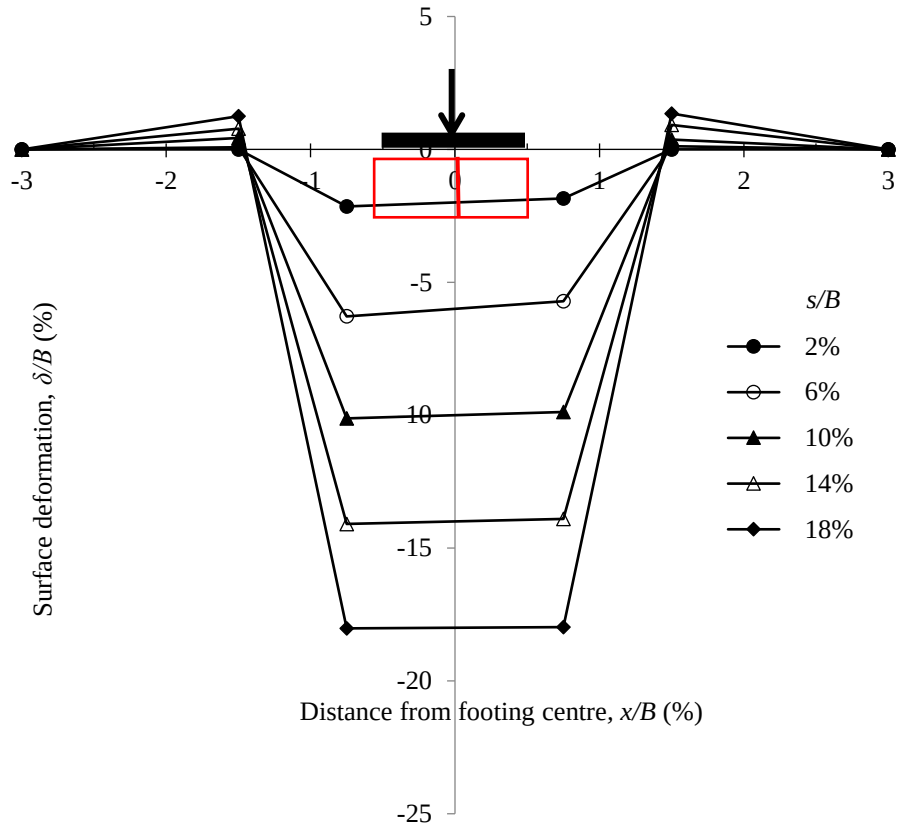
5
0
-3
-2
-1
0
1
2
3
-5
-10
-15
-20
-25
Surface deformation, δ/B (%)
Distance from footing centre, x/B (%)
s/B
2%
6%
10%
14%
18%

(a)

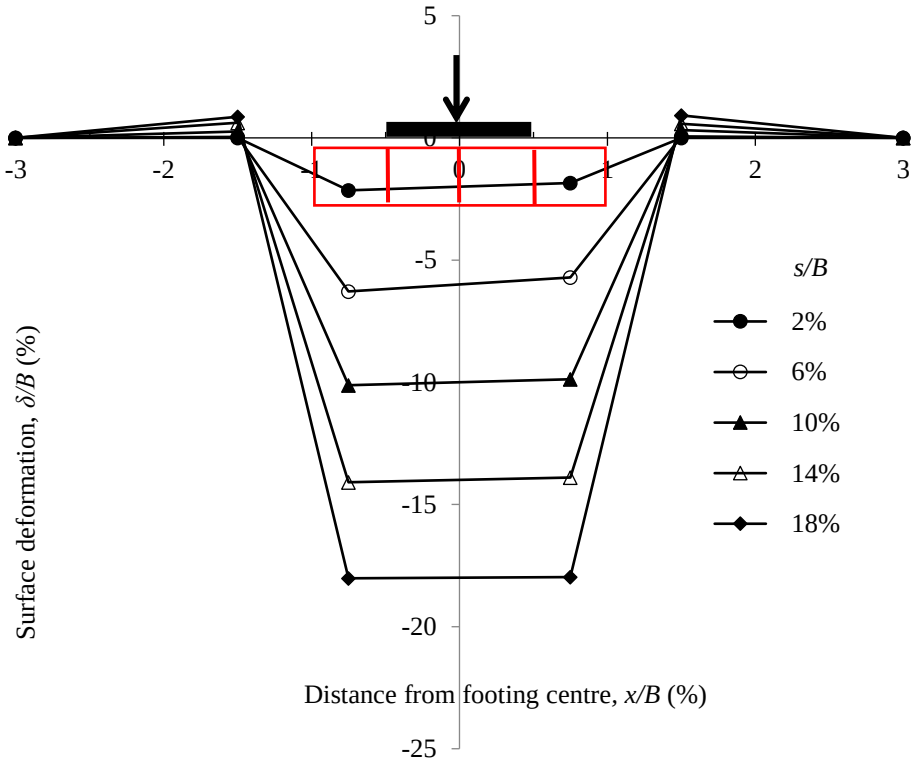
5
0
-3
-2
-1
0
1
2
3
-5
-10
-15
-20
-25
Surface deformation, δ/B (%)
Distance from footing centre, x/B (%)
s/B
2%
6%
10%
14%
18%

(b)

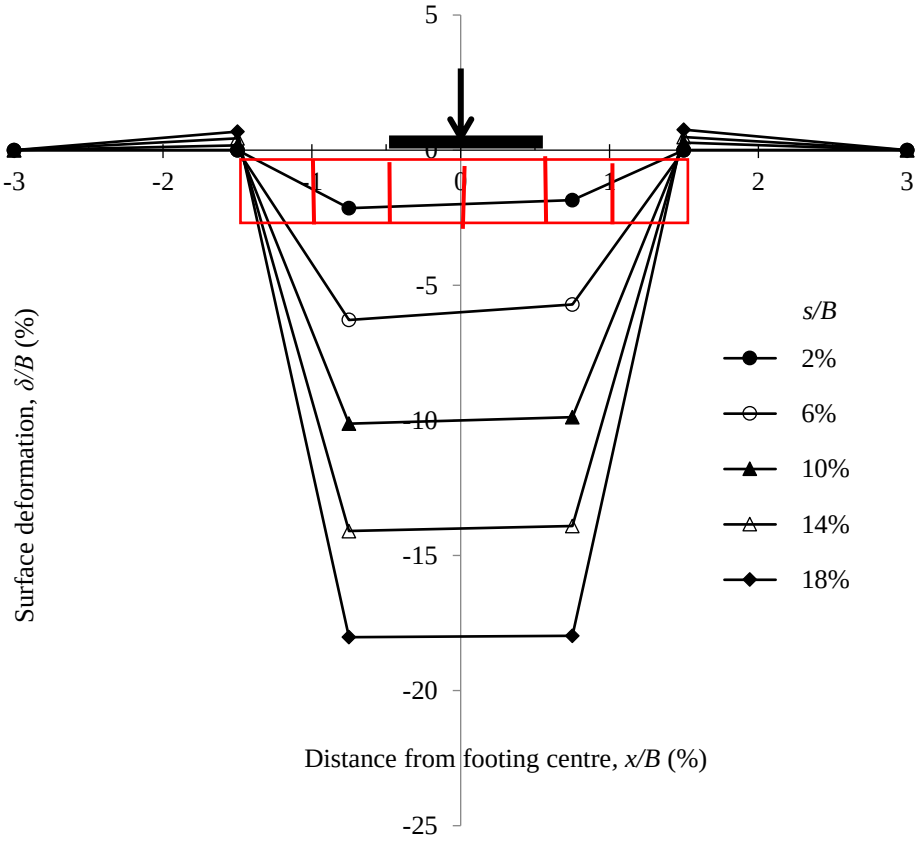
5
0
-5
-10
-15
-20
-25
-3
-2
-1
0
1
2
3
Surface deformation, δ/B (%)
Distance from footing centre, x/B (%)
s/B
2%
6%
10%
14%
18%

(c)

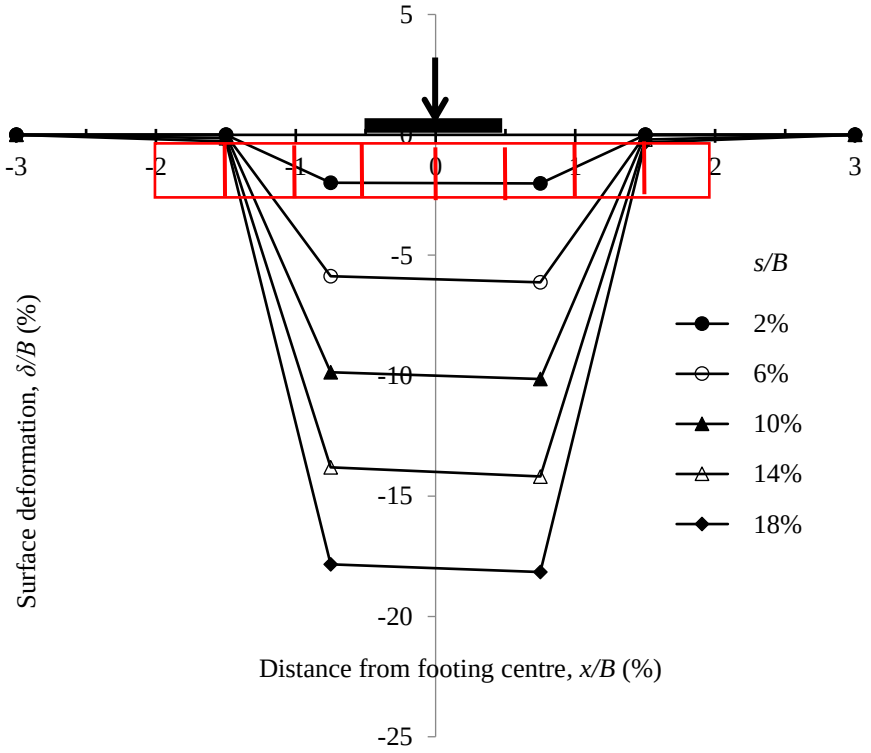
5
0
-5
-10
-15
-20
-25
-3
-2
-1
0
1
2
3
Surface deformation, δ/B (%)
Distance from footing centre, x/B (%)
s/B
2%
6%
10%
14%
18%

(d)

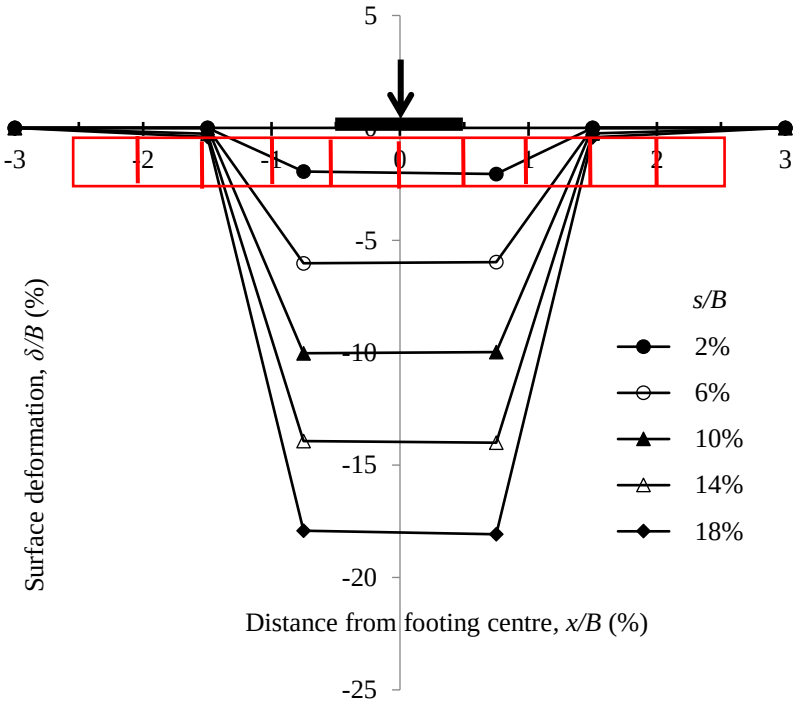

(e)

Fig. 4.35 Surface heaving with footing settlement for geocell-reinforced sand beds with geocell with d/B = 0.5, u/B = 0.1, h/B = 0.66, D_r = 70%, (a) b/B = 1; (b) b/B = 2; (c) b/B = 3; (d) b/B = 4; (e) b/B = 5.

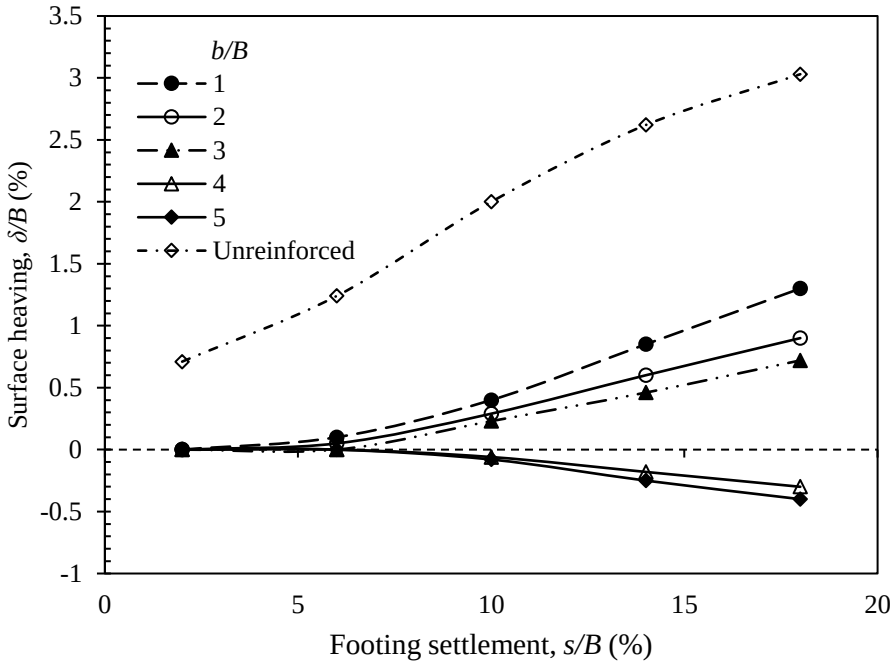

Fig. 4.36 Variation of surface deformations with footing settlement at a distance x = 1.5B from the centre of footing, for different width (b) of geocell reinforcement with geocell with u/B = 0.1, d/B = 0.5, h/B = 0.66, D_r = 70%.

4.3.6 Effect of variation of relative density of subgrade sand for 70% infill sand density ($D_{r,\,infill}$ = 70%)

Fig. 4.37(a-c) illustrates the effect of the relative density of subgrade sand (D_r) on the load-settlement behaviour of reinforced models corresponding to the geocell reinforcement width, test series F1 & G1 (Table 3.4), with $D_{r,\,infill}$ = 70%. Fig. 4.38 shows the variation of improvement factor with *b/B* at measured settlement *s/B* = 12% for different relative densities of subgrade sand. As can be seen, bearing-capacity generally increases as *b/B* values increase, but did not follow a linear trend with a rise in D_r. For instance, at *s/B* = 12%, *b/B* = 3, bearing-capacity Improvement Factor (*IF*) for D_r = 35% is 3.6, whereas the values are 2.5 and 2 for the reinforced models of D_r = 70 and 90%, respectively (Fig. 4.38).

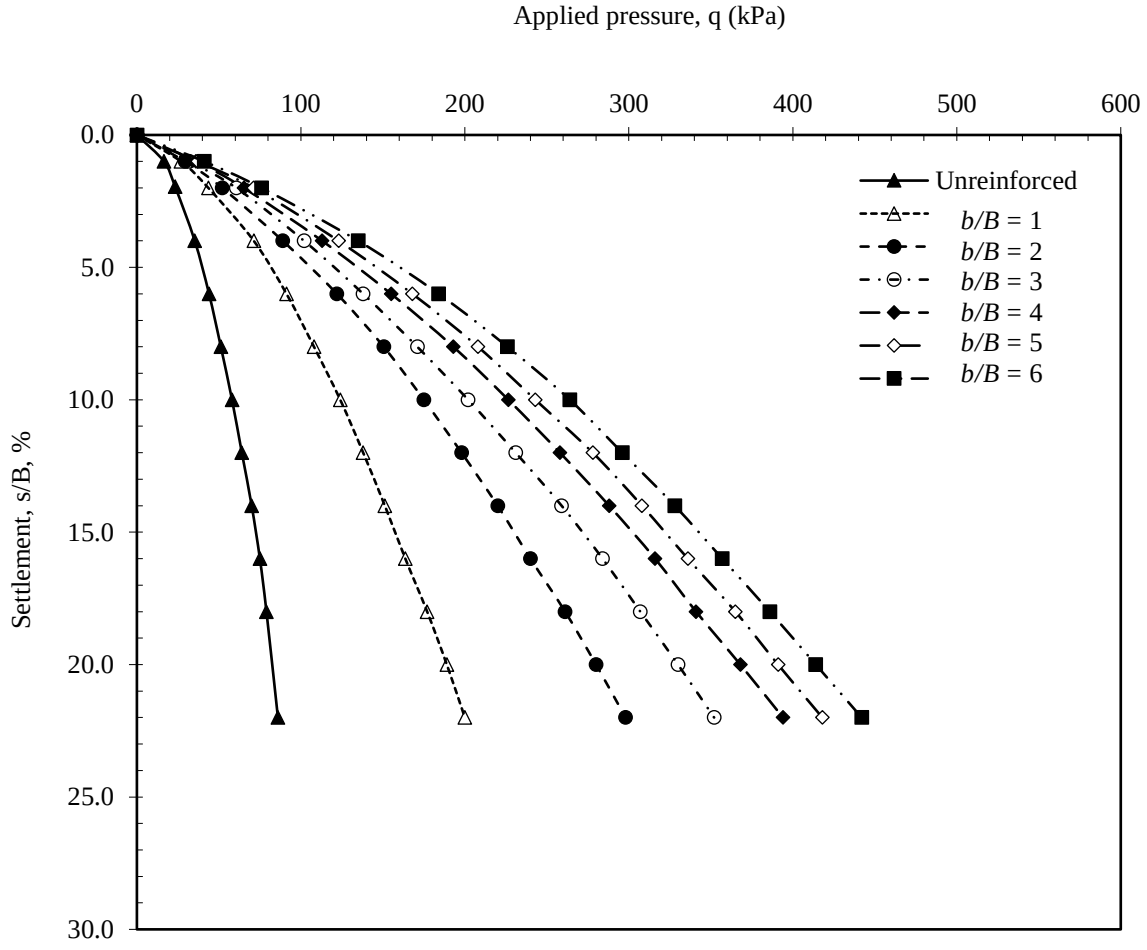

(a)

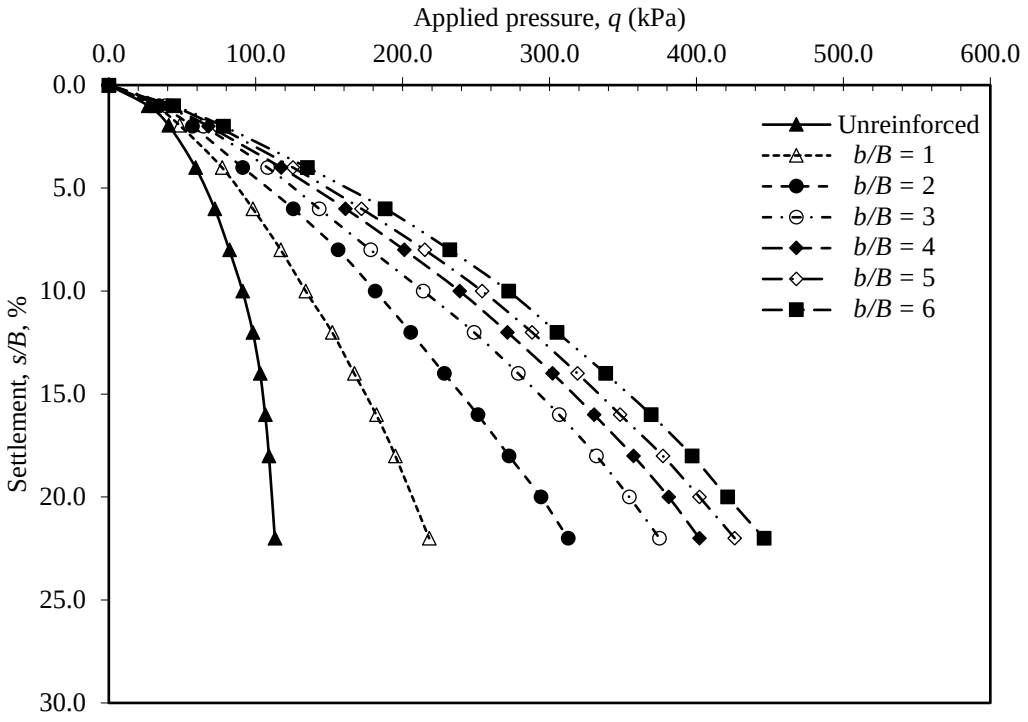

(b)

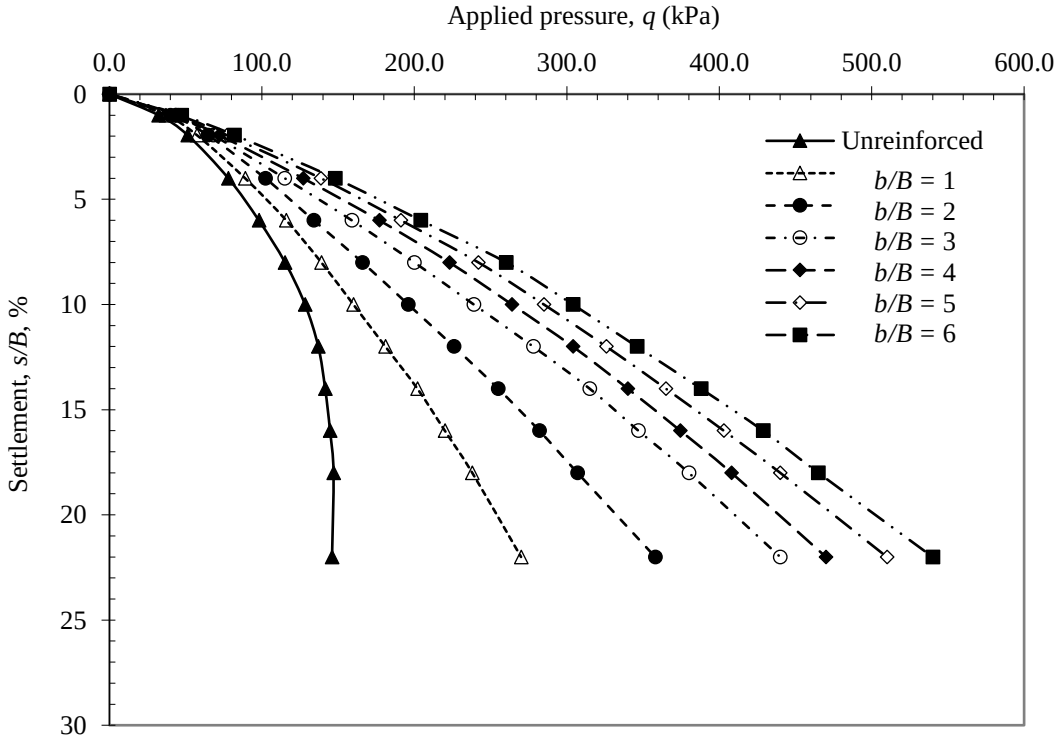

(c)

Fig. 4.37 Variation of footing settlement with bearing pressure for unreinforced and geocell-reinforced sand beds: (a) D_r = 35%; (b) D_r = 70%; and (c) D_r = 90%.

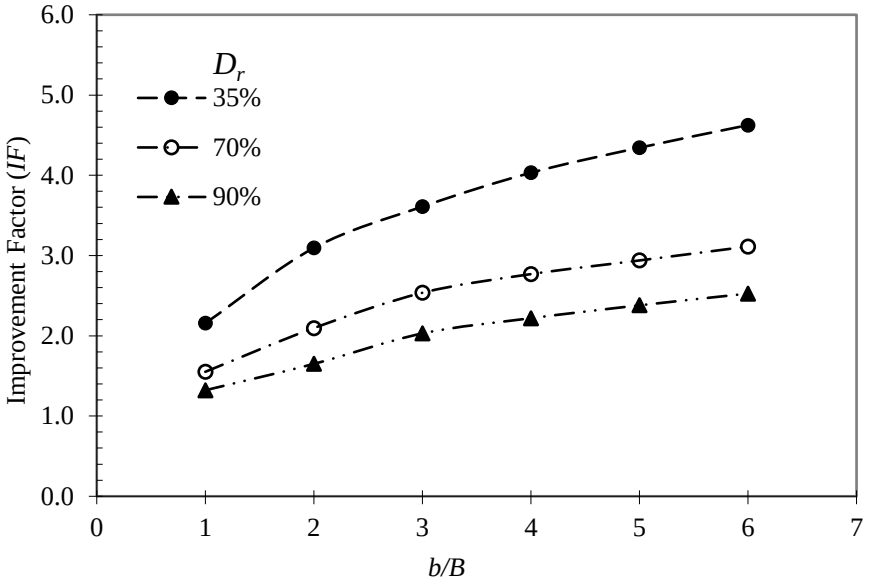

Fig. 4.38 Variation of Improvement factor with *b/B* at measured settlement *s/B* = 12% for different relative densities of subgrade sand.

The *PRS* value observed for different relative densities is shown in Fig. 4.39. A maximum *PRS* of about 81% was seen for loose sand (*Dr* = 35%), whereas it was about 68% for *Dr* = 70% and about 54% for *Dr* = 90% at *s/B* = 10%.

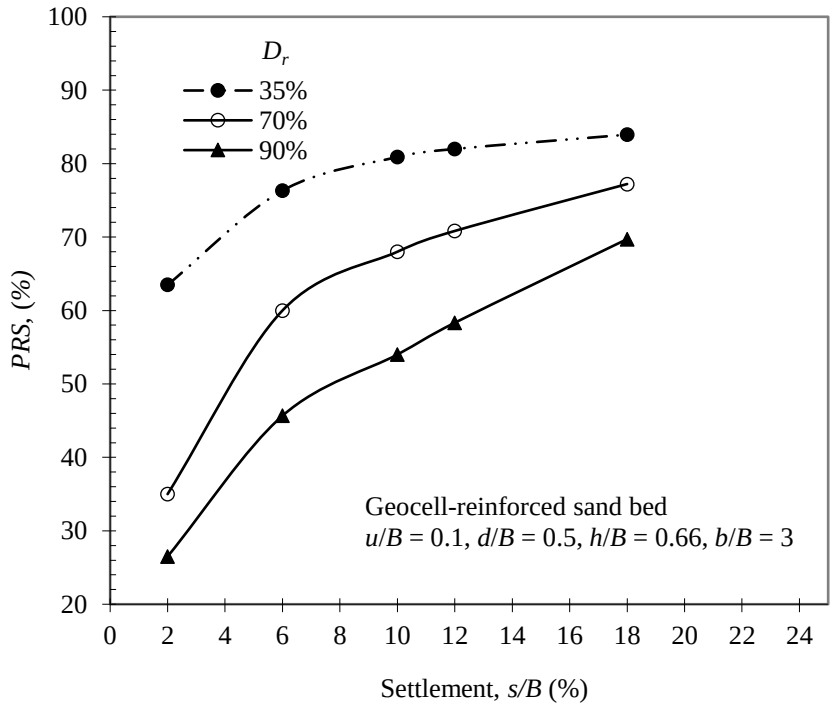

Fig. 4.39 *PRS* versus footing settlement for different relative densities, D_r = 35%, 70% & 90%

The variation of surface deformation with footing settlement for geocell-reinforced sand foundation, at a distance x = 1.5B from the centre of the footing, are presented in Figs. 4.40(a-c). The results, along with results in Fig. 4.8, depict that heaving is reduced in geocell-reinforced foundations with D_r = 70 and 90%, as compared to unreinforced foundations which are more predominant for the unreinforced case with D_r = 70 and 90%.

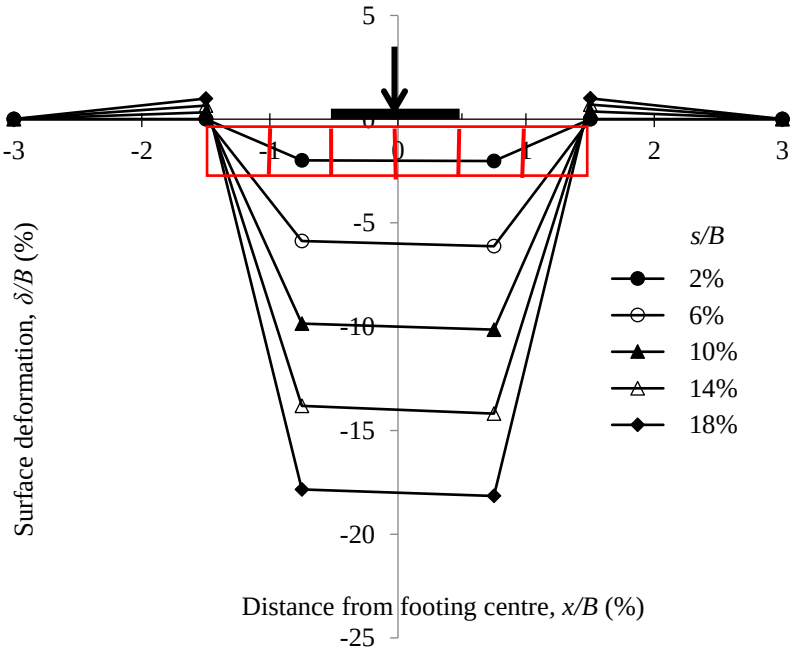

(a)

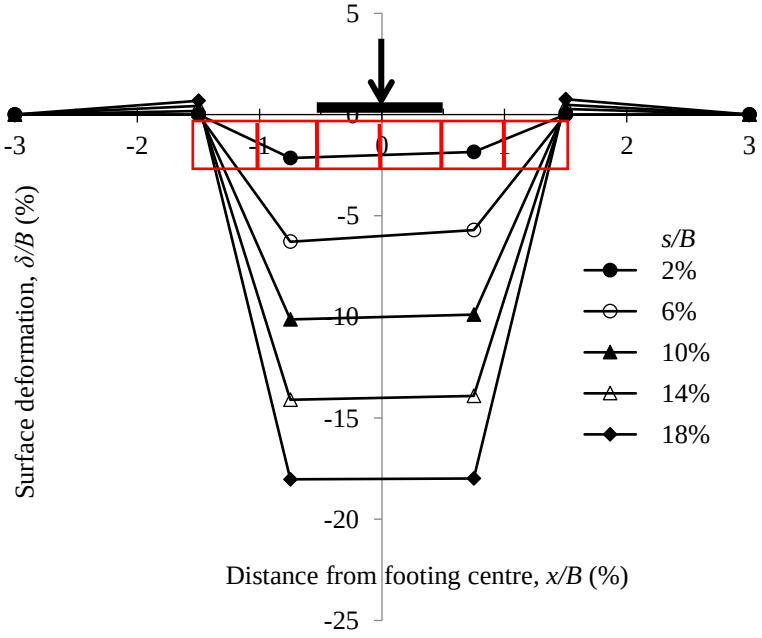

(b)

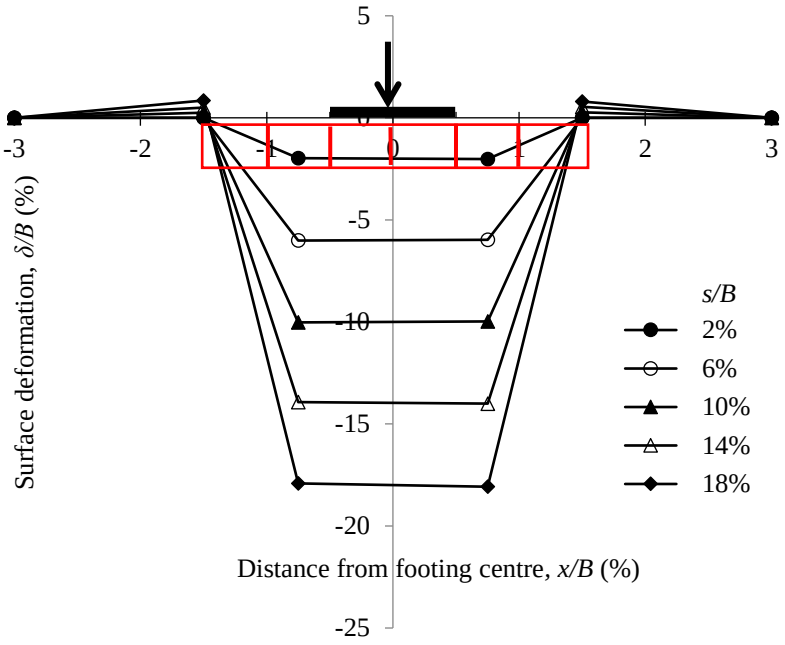

(c)

Fig. 4.40 Surface heaving with footing settlement for geocell-reinforced sand beds with geocell with d/B = 0.5, h/B = 0.66, u/B = 0.1, b/B = 3: (a) D_r = 35%; (b) D_r = 70%; (c) D_r = 90%.

For instance, the surface heaving of unreinforced sand with D_r = 90% at 18% of footing settlement is observed to be about 3.6% [Fig. 4.8(c)], whereas it reduces to about 0.8% with geocell reinforcement [Fig. 4.40(c)]. The reduction of heaving in geocell-reinforced foundations may be attributed due to the increase in the stiffness of geocell-reinforced sand layer because of which the footing loads distribute over a wider area and thus the underneath soil experiences a lower pressure. On the contrary, the surface heaving of geocell-reinforced sand with *Dr* = 35% is observed to increase to 1% at s/B = 18% from the corresponding value of 0.4% for unreinforced cases [Fig. 4.8(a)]. This may be because the geocell mattress act as a raft foundation and the failure envelope shifted to the edge of the geocell reinforcement instead of the edge of the square footing.

Fig. 4.41 shows the variation of the surface heaving and settlement of unreinforced and geocell-reinforced sand for different subgrade relative densities at equal load intensity of 79 kPa, which is the load-carrying capacity of unreinforced sand with D_r = 35% at s/B = 18% (Fig. 4.7). The result indicates a reduction of footing settlement with the provision of geocell reinforcement. A better load-carrying capacity of geocell-reinforced sand bed is

also observed as compared to the unreinforced sand. It is also observed that the depressions are greater at the centre and reduce towards the edge of the test tank which might be due to the bending of the geocell-sand mattress, as shown in Fig. 4.42(a-b). Furthermore, the maximum depth of depressions at the centre is found to reduce as the subgrade relative density increases. Similar deformation responses of reinforced foundation systems have also been reported by Biswas et al. [12], Dash et al. [23, 29], and Sireesh et al. [115] when geocells made from geogrids were used.

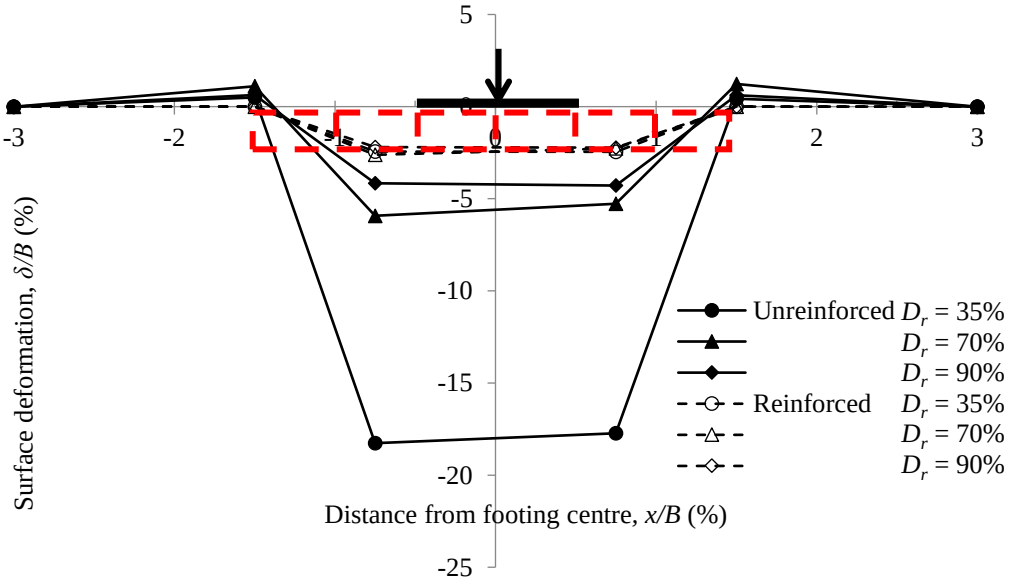

Fig. 4.41 Variation of surface heaving and settlement for unreinforced and geocell-reinforced sand beds at an equal intensity of load for different subgrade relative density, D_r = 35%, 70%, and 90%.

(a)

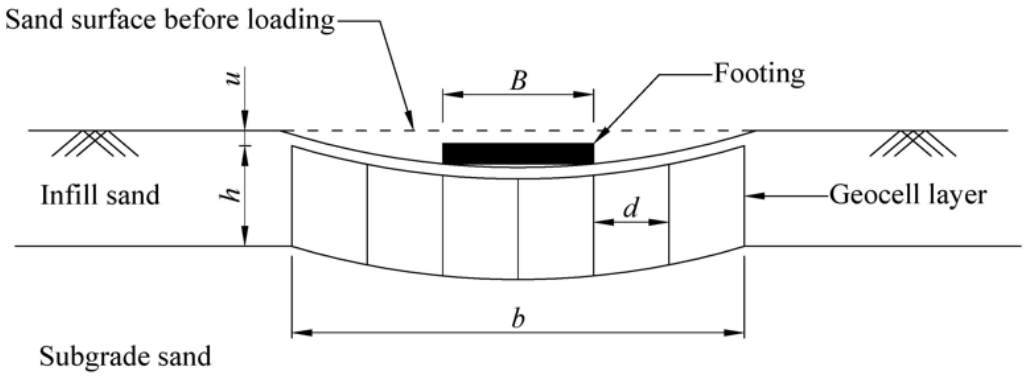

Section at A-B

(b)

Fig. 4.42 Photographic view of footing settlement for (a) geocell-reinforced foundations (d/B = 0.5, h/B = 0.66, u/B = 0.1, b/B = 3 & $D_{r,}$ = 70%); (b) Schematic diagram of settlement of geocell-reinforced foundation system along section A-B.

4.3.7 Effect of relative density of infill sand

Bearing pressure versus settlement response of unreinforced sand (D_r = 70%) and geocell-reinforced sand with different infill soil densities are shown in Fig. 4.43, test series H (Table 3.4).

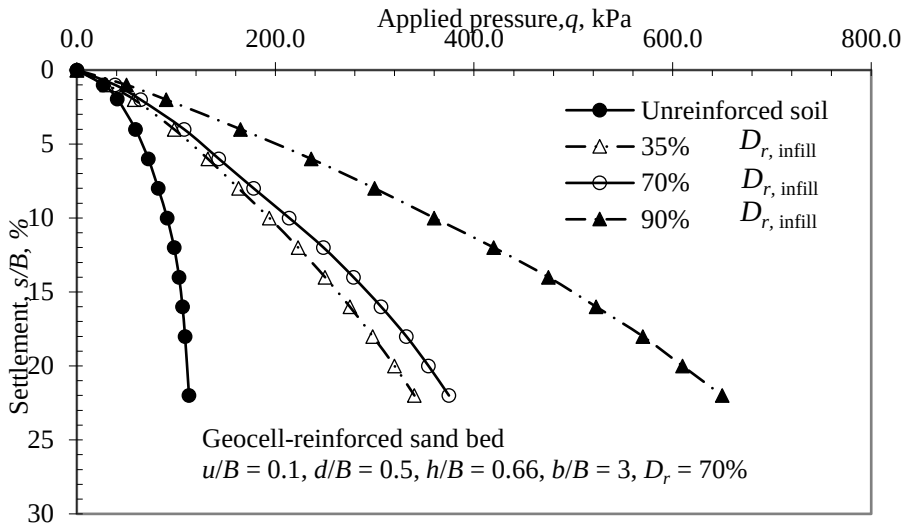

Fig. 4.43 Variation of settlement with bearing pressure for varying infill density of geocell-reinforced sand beds supported on subgrade sand D_r = 70%.

The results show that great improvement in bearing capacity and settlement response can be achieved by increasing the relative density of infill soil. Fig. 4.44 represents the variation of the bearing capacity improvement factor (*IF*) versus settlement for different relative densities of infill soil ($D_{r,\,infill}$). It can be seen that the higher the infill density of soil in the geocells better is the corresponding improvement factor. The test results show that *IF* increases 3.0, 3.3, and 5.8 folds at settlement *s/B* = 22% for relative density of 35%, 70%, and 90%, respectively. This observation points to a mechanism where the frictional stress between infill soil and geocell provides additional strength to the reinforced soil. The loose infill soil consumes the applied displacement in the readjustment of the void space thereby inducing lesser frictional drag along the soil-geocell interface. On the other hand, in soil with an increase in density, there is less redistribution of void space and consequently, there is a tendency for expansion of infill soil under loading. This leads to the mobilization of shear resistance along the soil-geocell interface and the improvement of the capability of the soil with geocell to carry the load. Dash [21] has also reported a similar observation when geocells made from geogrid were used.

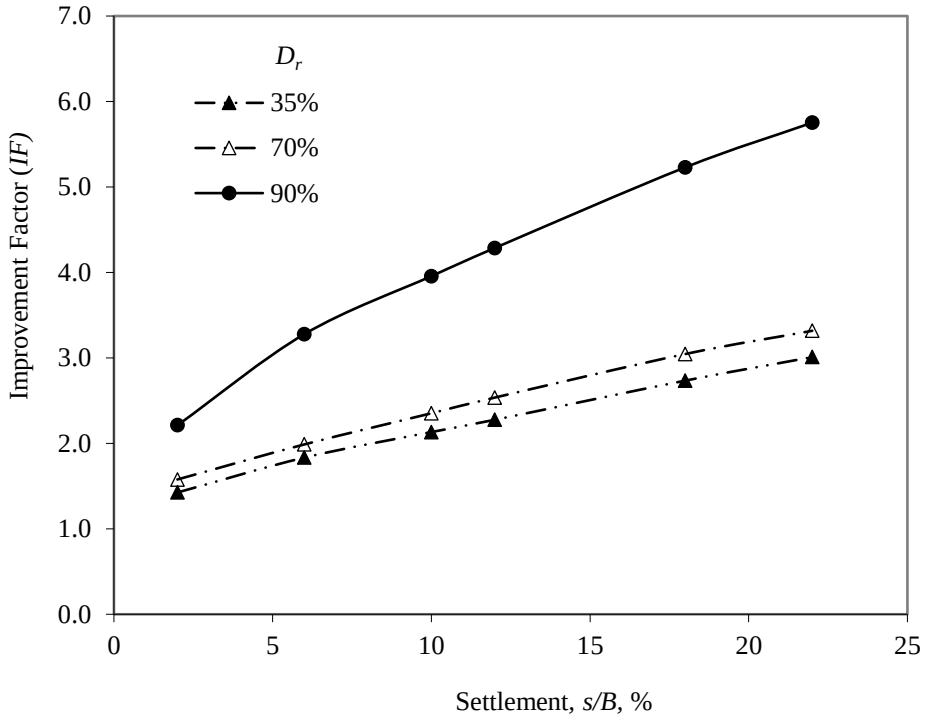

Fig. 4.44 Variation of *IF* with footing settlement for different infill soil density in the geocell pockets

The variation of *PRS* at different levels of footing settlement (*s/B*) for different infill soil densities in geocell pockets is plotted in Fig. 4.45. The curves indicate that the *PRS* value increases as the infill soil density increases. The test results illustrate that *PRS* values increase by approximately 63%, 68%, and 80% for infill soil density of 35%, 70%, and 90%, respectively, due to the inclusion of geocell reinforcement at *s/B* = 10%, i.e. 63%, 68% and 80% reduction in settlement of the geocell-reinforced sand beds as compared to unreinforced sand bed having 70% relative density.

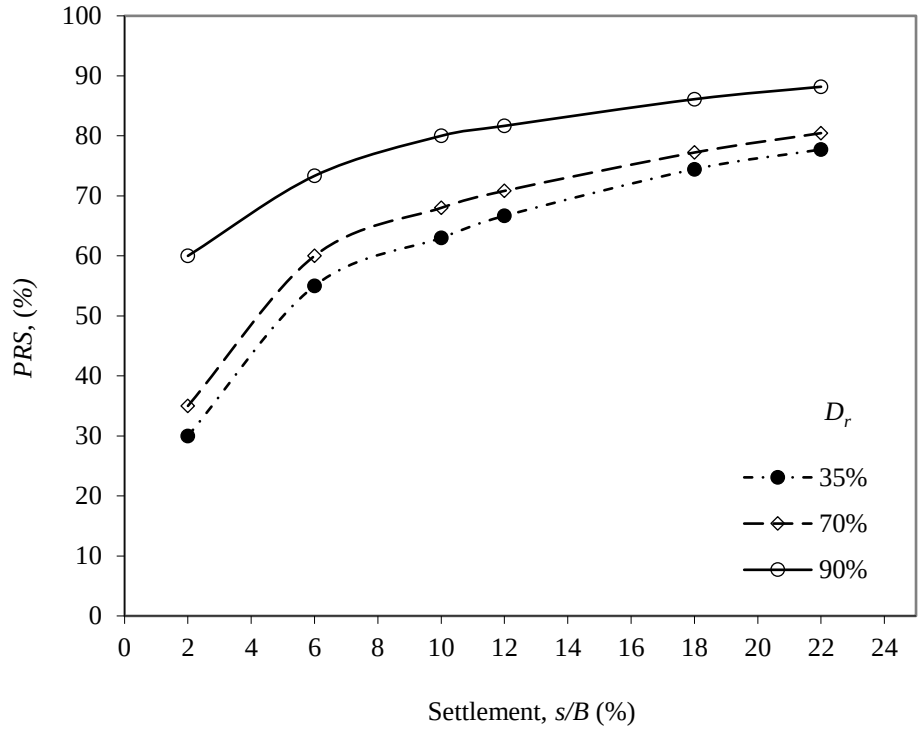

Fig. 4.45 Variation of the percentage reduction in settlement (*PRS*) with footing settlement for different infill soil density

4.4 Summary

The results of several laboratory model load tests carried out to investigate the effect of various parameters such as the effect of the shape of footing, the relative density of sand subgrade, geocell geometric dimensions, and relative density of infill sand (in the geocells) subjected to static load have been reported. Three types of footing such as square, rectangular, and strip footings are used to investigate the effect of the shape of footing on unreinforced and geocell-reinforced sand foundations with geocell with *d/B* =

0.5, h/B = 0.66, u/B = 0.1, b/B = 3 & $D_{r,}$ = 70%. Thereafter, a series of laboratory model load tests are carried out to investigate the influence of various parameters such as relative density of sand subgrade (D_r), geocell placement depth from the base of the footing (u), the equivalent diameter of geocell pocket (d), the height of geocell reinforcement (h), the width of geocell reinforcement (b) and relative density of infill sand in the geocells ($D_{r,\ infill}$) on the bearing capacity of geocell reinforced sand foundations under the square footing. Based on the test results and within the parameters studied, the following conclusions are drawn:

- In unreinforced sand beds, local failure modes are observed for the square and rectangular types of footing. However, a general type of failure mode is noticed for strip footing. This is attributed due to different ways of strain localization in the ground for both the 3D and 2D cases. On the contrary, for the geocell-reinforced sand beds, no clear failure modes are observed for all three types of footings even up to a large settlement of s/B = 22%. Further, the bearing capacity *IF* increases by 2.4, 2.3, and 1.9 folds for square, rectangular, and strip footing, respectively, due to the inclusion of geocell reinforcement at s/B = 10%. The higher performance improvement of bearing capacity in square and rectangular footing as compared to strip footing is due to the 3D failure mechanism in square/rectangular footing and the 2D failure mechanism for strip footing.

- The improvement in bearing capacity decreases with an increase in the denseness of the sand bed. In the case of a geocell-reinforced foundations system with a low-density sand bed (D_r = 35%), maximum improvement is found about 3.5 times, whereas it is only 1.9 times for higher density sand bed (D_r = 90%) at s/B = 10%. Thus, it can be concluded that the geotextile-based geocell contribution in improving the load-carrying capacity is very significant for low relative density sand beds. Furthermore, the use of geotextile-based geocell reinforcement almost arrests the surface heaving of soil irrespective of which relative density of sand bed the footing has been rested.

- It can be said that the critical depth of placement of the geocell reinforcement layer (u) giving maximum performance improvement is about $0.1B$ from the base of the footing.

- In general, the performance improvement in bearing capacity increases with a reduction in the geocell's pocket size (d). However, when the footing size is larger than the geocell pocket size, the performance improvement is substantially high. Further, heaving of the soil surface is more predominant for a geocell pocket size higher than the footing size. Thus, for all practical applications, the geocell reinforcement layer and footing should be designed such that the footing completely covers at least one geocell pocket opening.

- It is noted that the performance improvement of bearing capacity increases with an increase in the geocell mattress height. However, the efficacy of improvement is marginal beyond h/B =0.66. Moreover, the surface heaving of the soil surface reduces with the increase in height of geocell reinforcement.

- The bearing capacity improvement factor increases with an increase in the geocell reinforcement width. However, when reinforcement width reaches an optimum value ($3B$), the effects of improvements become marginal. Besides, surface heaving on the soil surface reduces with an increase in the width of geocell reinforcement.

- It can be said that the higher density of the infill soil imparts more capability to the sand bed with geocell reinforcement in terms of bearing load and resisting settlement. The bearing capacity improvement factor increases from 2.4 to 4 at s/B = 10% for the relative density of infill soil from 70% to 90%. It is, therefore, concluded that the highest possible compaction of the infill soil is key to achieving the effective performance of geocell reinforcement of soil.